

## Modeling and measuring the effects of disturbance history and climate on carbon and water budgets in evergreen needleleaf forests

P.E. Thornton<sup>a,\*</sup>, B.E. Law<sup>b</sup>, Henry L. Gholz<sup>c</sup>, Kenneth L. Clark<sup>c</sup>, E. Falge<sup>d</sup>,  
D.S. Ellsworth<sup>e</sup>, A.H. Goldstein<sup>f</sup>, R.K. Monson<sup>g</sup>, D. Hollinger<sup>h</sup>,  
M. Falk<sup>i</sup>, J. Chen<sup>j</sup>, J.P. Sparks<sup>g</sup>

<sup>a</sup> *Climate and Global Dynamics Division, National Center for Atmospheric Research, 1850 Table Mesa Dr., Boulder, CO 80305, USA*

<sup>b</sup> *328 Richardson Hall, Oregon State University, Corvallis, OR 97331-5752, USA*

<sup>c</sup> *School of Forest Resources and Conservation, University of Florida, Gainesville, FL 32611, USA*

<sup>d</sup> *Pflanzenökologie, Universität Bayreuth, 95440 Bayreuth, Germany*

<sup>e</sup> *School of Natural Resources and Environment, 430 E. University Ave., University of Michigan, Ann Arbor, MI 48109-1115, USA*

<sup>f</sup> *ESPM, University of California, Berkeley, CA 94704, USA*

<sup>g</sup> *Department of Environmental, Population, and Organismic Biology, Campus Box 334, University of Colorado, Boulder, CO 80309-0334, USA*

<sup>h</sup> *USDA Forest Service, 271 Mast Road, Durham, NH 03824, USA*

<sup>i</sup> *Atmospheric Science Group, LAWR, 122 Hoagland Hall, University of California, Davis, CA 95616, USA*

<sup>j</sup> *Landscape Ecology and Ecosystem Science, Earth, Ecological and Environmental Sciences, University of Toledo, Toledo, OH 43606-3390, USA*

Accepted 3 April 2002

### Abstract

The effects of disturbance history, climate, and changes in atmospheric carbon dioxide (CO<sub>2</sub>) concentration and nitrogen deposition (N<sub>dep</sub>) on carbon and water fluxes in seven North American evergreen forests are assessed using a coupled water–carbon–nitrogen model, canopy-scale flux observations, and descriptions of the vegetation type, management practices, and disturbance histories at each site. The effects of interannual climate variability, disturbance history, and vegetation ecophysiology on carbon and water fluxes and storage are integrated by the ecosystem process model Biome-BGC, with results compared to site biometric analyses and eddy covariance observations aggregated by month and year. Model results suggest that variation between sites in net ecosystem carbon exchange (NEE) is largely a function of disturbance history, with important secondary effects from site climate, vegetation ecophysiology, and changing atmospheric CO<sub>2</sub> and N<sub>dep</sub>. The timing and magnitude of fluxes following disturbance depend on disturbance type and intensity, and on post-harvest management treatments such as burning, fertilization and replanting. The modeled effects of increasing atmospheric CO<sub>2</sub> on NEE are generally limited by N availability, but are greatly increased following disturbance due to increased N mineralization and reduced plant N demand. Modeled rates of carbon sequestration over the past 200 years are driven by the rate of change in CO<sub>2</sub> concentration for old sites experiencing low rates of N<sub>dep</sub>. The model produced good estimates of between-site variation in leaf area index, with mixed performance for between- and within-site variation in evapotranspiration. There is a model bias

\* Corresponding author. Tel.: +1-303-497-1727; fax: +1-303-497-1348.

E-mail address: thornton@ucar.edu (P.E. Thornton).

toward smaller annual carbon sinks at five sites, with a seasonal model bias toward smaller warm-season sink strength at all sites. Various lines of reasoning are explored to help to explain these differences.

© 2002 Elsevier Science B.V. All rights reserved.

*Keywords:* Net ecosystem exchange; Ecosystem respiration; Carbon dioxide concentration; Nitrogen deposition; Eddy covariance; Ecosystem model; Carbon budget; Water budget; Nitrogen budget; Evergreen needleleaf forest

## 1. Introduction

The exchanges of carbon, water and energy between vegetation and the atmosphere are important determinants of regional climate and global carbon budgets (Denning et al., 1995; Schimel et al., 1996). While forests occupy ~30% of the earth's land surface, and account for 80–90% of all plant carbon, their contribution to the global carbon budget is uncertain. Factors that influence processes controlling net carbon uptake include physiological differences in forest functional groups and developmental stages, time since disturbance, management practices, climate, and nutritional status. Field studies on whole ecosystem carbon dioxide and water vapor exchange, coupled with small-scale studies of biological processes, and evaluation with ecosystem process models have helped us bridge the gap between organismal, stand and regional understanding of processes.

Numerical models of the carbon, water and nitrogen budgets could provide a means of estimating the spatial and temporal details of changes in carbon storage (McGuire et al., 1992, 2001; Kucharik et al., 2000; Schimel et al., 2000). One possible evaluation of such models is to test their ability to explain the within-site and between-site variability in flux measurements across networks such as AmeriFlux. We recently compared eddy covariance flux measurements, biometric carbon budget measurements, and modeled carbon budgets for an evergreen site in Oregon, and found that biometric and model estimates of NEE and its components were in good agreement, but that these methods both gave smaller estimates of the net carbon sink at the site than provided by eddy covariance measurements (Law et al., 2001c). This study suggested that additional comparisons in different climates and for stands at different developmental stages might help to explain the discrepancies between modeled and observed fluxes.

This paper focuses on evergreen coniferous forests that are part of the AmeriFlux network of sites where physiological, ecological and micrometeorological measurements are being made to understand processes controlling carbon dioxide and water vapor exchange with the atmosphere. The forests in this study cover a broad range in climate and growth form, including Rocky Mountain high-elevation spruce, boreal spruce forests in the northeastern US, semi-arid temperate ponderosa pine and wet temperate Douglas-fir in the Pacific northwest US, mild temperate loblolly pine in the southeastern US, and subtropical slash pine plantations in central Florida. The selected sites also include a wide range in the time since disturbance, from recently harvested plantation stands to old-growth forests.

We use eddy covariance measurements, biometric analysis, and modeling to investigate controls on net carbon uptake in these forests. We apply the model Biome-BGC, using site-specific parameters where available, to estimate gross photosynthesis, net primary production, total ecosystem respiration, net ecosystem production, and transpiration. Our purpose is to test the ability of the model to explain between-site differences and within-site seasonal dynamics in carbon and water budgets, and to evaluate the influence of site history, developmental stage, and climate on these ecosystem processes. The use of a coupled water–carbon–nitrogen model is important because it allows us to evaluate multiple simultaneous constraints on model behavior. It also provides a logically consistent set of model estimates for water and carbon fluxes and state variables that can be used to make inferences about possible causes for discrepancies between model results and observations. We use ancillary biological measurements from several sites to help to explain discrepancies between the model estimates and flux measurements where they occur. This study is part of an ongoing interaction intended to improve our ability to both measure and model

the dynamics of the terrestrial carbon cycle, increasing our understanding of the interactions between climate, vegetation, and natural and human-induced disturbances.

## 2. Methods

### 2.1. Site descriptions

This study is a synthesis of data on evergreen coniferous forests where CO<sub>2</sub> and H<sub>2</sub>O exchange measurements have been made above the canopy, together with a variety of biological measurements. The sites

are part of the AmeriFlux and FLUXNET networks of sites. The sites cover a broad range of climate, with annual total precipitation from 80 to 230 cm per year, and average annual temperature from 2 to 22 °C. Taken together the sites are fairly representative of the distribution of evergreen needleleaf forests within the conterminous United States (Fig. 1). General characteristics of the sites used in this study are shown in Table 1, which also lists the site abbreviations used in subsequent text, tables and figures.

We are particularly interested here in the unique history of disturbance at each site, including the timing and intensity of natural disturbances such as fire, and the timing and details of managed disturbances

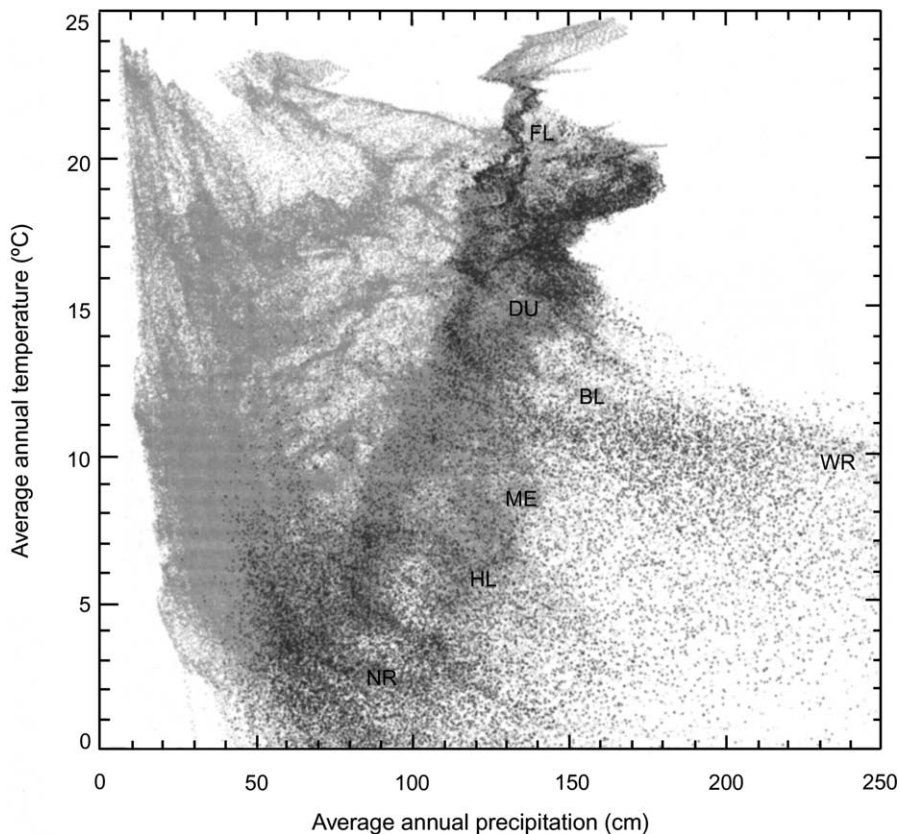


Fig. 1. Distribution of study sites in mean annual climate space. Climate parameters are the annual total precipitation (x-axis) and the annual average air temperature (y-axis) taken over an 18-year period of record (1980–1997), from the Daymet database. Light gray points indicate the climate space distribution of landmass within the conterminous United States, and dark gray points highlight the subset of evergreen needleleaf forest types. Original landcover information is at 1 km resolution, from the University of Maryland Global Landcover Facility (Hansen et al., 2000). Both landcover and climate data have been resampled to 10 km resolution for plotting points in this figure. Symbols show the location in climate space of each of the seven sites, using climate data from the Daymet database for the 1 km gridcell nearest to the specified geographic location for the site.

Table 1  
Site characteristics<sup>a</sup>

Site (symbol)	Location	Elevation (Daymet) (m)	$T_{\text{ann}}$ (S.D.) (°C)	$T_{\text{grow}}$ (S.D.) (°C)	$P_{\text{ann}}$ (S.D.) (mm)	$P_{\text{grow}}$ (S.D.) (mm)	Sand (%)	Silt (%)	Clay (%)	Historic $N_{\text{dep}}$ (g N m <sup>-2</sup> per year)	Current $N_{\text{dep}}$ (g N m <sup>-2</sup> per year)
Blodgett forest, CA (BL)	38°54'N, 120°38'W	1315 (1280)	11.6 (0.7)	16.4 (1.0)	1493 (525)	218 (99)	30	35	35	0.22	0.22
Duke forest, NC (DU)	36°2'N, 79°8'W	163 (230)	14.6 (0.6)	21.2 (0.6)	1260 (190)	633 (118)	43	46	11	0.18	0.50
Slash pine plantation, Gainesville, FL (FL)	29°44'N, 82°9'W	50 (42)	20.6 (0.5)	25.0 (0.4)	1334 (179)	777 (168)	94	5	1	0.19	0.30
Howland forest, ME (HL)	45°12'N, 68°44'W	60 (122)	5.5 (0.6)	14.0 (0.5)	1134 (169)	596 (105)	30	40	30	0.16	0.29
Metolius, OR (ME)	44°30'N, 121°37'W	915 (901)	8.2 (0.7)	13.3 (0.7)	1251 (327)	313 (78)	62	30	8	0.18	0.18
Niwot ridge, CO (NR)	40°2'N, 105°33'W	3050 (2992)	2.1 (0.5)	8.0 (0.7)	808 (132)	431 (100)	70	20	10	0.12	0.30
Wind river, WA (WR)	45°49'N, 121°57'W	355 (400)	9.4 (0.7)	14.3 (0.7)	2247 (453)	499 (116)	40	30	30	0.32	0.32

<sup>a</sup> Elevation parameters are given for both the site and the nearest 1 km Daymet gridcell when available. Climate parameters are from the nearest Daymet gridcell, and include the interannual standard deviation from the 18-year Daymet record. Climate parameters include annual average air temperature ( $T_{\text{ann}}$ ), growing season average air temperature ( $T_{\text{grow}}$ ), annual total precipitation ( $P_{\text{ann}}$ ), and growing season precipitation ( $P_{\text{grow}}$ ). Growing season is defined as year-days 90–270. Values of mineral nitrogen deposition ( $N_{\text{dep}}$ , from nitrate and ammonia) are given for both historical conditions, estimated circa 1795 as a function of  $P_{\text{ann}}$ , and current conditions, estimated from the NADP network.

Table 2  
Current vegetation age structure and site disturbance history<sup>a</sup>

Site	Current age (years)	Disturbance history
BL	10	1990: clear-cut (99.9%), replanted with initial leaf C of 10 g C m <sup>-2</sup>
DU	17	1983: clear-cut (99.9%), slashburned (25%), replanted with initial leaf C of 10 g C m <sup>-2</sup>
FL	10	1990: clear-cut (99%), slashburned (99%), replanted with initial leaf C of 10 g C m <sup>-2</sup>
HL	90	1910: selective harvest (75%)
ME	45–250 (three age classes)	1750: stand-replacing fire (99%); 1850: fire (25%); 1950: fire (25%)
NR	95	1905: harvest (99%)
WR	0–500 (many age classes)	1550: stand-replacing fire (99%); 1550–present: continuous whole-plant mortality (0.5% per year) and continuous low-level fire (1% per year)

<sup>a</sup> For all sites, the disturbance history includes changes in atmospheric CO<sub>2</sub> and N<sub>dep</sub> starting from 1795. Percentage in parentheses indicates the fraction of the stand biomass affected.

such as harvest, slashburning and replanting. The disturbance history at each site, as communicated by the site Principal Investigator, is summarized in Table 2. We also considered the effects of measured changes in the concentration of atmospheric CO<sub>2</sub> and deposition of mineral nitrogen (N<sub>dep</sub>), as well as the interaction of these gradual environmental changes with the episodic disturbance histories.

The Howland forest (HL) is located about 35 miles north of Bangor, Maine. The natural stands in this boreal-northern hardwood transition forest consist of ~41% red spruce (*Picea rubens* Sarg.), 25% eastern hemlock (*Tsuga canadensis* (L.) Carr.), 23% other conifers (primarily balsam fir (*A. balsamea* (L.) Mill.), white pine (*P. strobus*, L.), and northern white cedar (*Thuja occidentalis* L.)), and 11% hardwoods (red maple (*Acer rubrum* L.), paper birch (*Betula papyrifera* Marsh.)). The soils are generally glacial tills with low fertility and high organic composition. The forest was logged selectively around 1910.

The Duke Forest (DU) is in Orange County, NC. The climate is warm and humid, with mild winters and an average frost-free season of 200 days. The site is loblolly pine (*P. taeda*), planted in 1983 following clearing and burning the previous year. The soils are ultic hapludalf.

The Florida site (FL) is located 15 km northeast of Gainesville, FL. It is an even-aged slash pine (*Pinus elliottii*) pulpwood plantation. The stand was planted in 1990 at harvest density following harvest of the previous stand (stems only), chopping, broadcast burning, bedding and herbicide application for weed control. The stand has not been fertilized or thinned since establishment. The understory vegetation is pri-

marily evergreen, and consists of *Serenoa repens*, *Ilex glabra* (L.) A. Gray, and *Myrica cerifera* L. The soils are ultic alaquods that are poorly drained and low in organic matter.

Four sites are in the western US, characterized by a wet-winter, dry-summer climate. These are the Metolius (ME) old ponderosa pine (*P. ponderosa*) site in Oregon, the Wind River (WR) Douglas-fir/western hemlock (*Pseudotsuga menziesii*/*Tsuga heterophylla*) old-growth site in Washington, the Blodgett Forest (BL) young ponderosa pine plantation in California, and the Niwot Ridge (NR) subalpine conifer forest in Colorado.

The ME old ponderosa pine forest is about 15 km west of Sisters, Oregon, located in the Metolius Research Natural Area. It has never been logged. The site consists of about 27% old trees (~250 years) assumed to have regenerated following a stand-replacing fire in about 1750, 25% younger trees (~50 years) and 48% mixed-age trees. The understory is sparse. The younger trees are the first successful cohort since fire exclusion began ~100 y.b.p. The soils are alfic vitrixerands.

The WR forest is estimated to be 400–500 years, having originally regenerated following a stand-replacing fire in about 1550. The occurrence and severity of fires since 1550 is unknown. Two fires burned in the area, in 1902 and 1929, but there is argument over the effects of these fires within the flux tower footprint (J. Chen, personal communication). It is a multi-layered canopy with different age classes of trees in the understory and in canopy gaps formed by windthrow and mortality. The canopy species composition is very diverse, but the dominant

species are Douglas-fir and western hemlock. Associated species include western red-cedar (*Thuja plicata* Donn.), western white pine (*P. monticola* Dougl.), Pacific silver fir (*A. amabilis* (Dougl.) Forb.), grand fir (*A. grandis* (Dougl.) Lindl.) and noble fir (*A. procera* Rehd.).

The BL site is a ponderosa pine plantation established following a clear-cut in 1990 (planting density 1200 trees per hectare). Average canopy height is 3 m. Other trees and shrubs make up less than 30% of the site biomass. The soil is loam to clay-loam, and classified as a mesic ultic haploxeralf in the Cohasset series, with andesitic lahar parent material. Organic matter content and total nitrogen in the top 30 cm are 6.9 and 0.17% by weight, respectively. Winters are wet and cool and summers are warm and dry, with almost no precipitation in mid-summer.

The NR site is in a subalpine forest just below the Continental Divide near Nederland, CO. The forest was established from natural regrowth after extensive logging from 1900 to 1910. The forest surrounding the tower is composed of subalpine fir (*Abies lasiocarpa*), Engelmann spruce (*Picea engelmannii*), and lodgepole pine (*Pinus contorta*). The understory is relatively sparse, containing tree seedlings from all three species and patches of *Vaccinium myrtillus* (25% average cover). The forest slopes gently (6–7%) and uniformly, decreasing from west to east. Subalpine forest extends 2 km west of the tower, where it forms a Krumholz, treeline ecotone that ultimately blends into alpine tundra.

## 2.2. Biological measurements

Biological measurements were made in previous studies, but we briefly describe them here. Maximum seasonal one-sided leaf area index (LAI) was estimated from optical measurements or the product of annual litterfall, leaf longevity, and mean specific leaf area (SLA,  $\text{cm}^2 \text{g}^{-1}$ ). At ME optical measurements were made using LAI-2000s (LICOR, Lincoln, NE), and the data were corrected for clumping of foliage within shoot, and clumping at scales larger than shoot (Law et al., 2001a,b). The LAI-2000 was also used at DU, but values were not corrected for foliage clumping, so they may be slightly low in comparison. At HL the LAI-2000 measurements made in 1998 were corrected for clumping by using a correction factor of

1.5 (Fassnacht et al., 1994; Stenberg, 1996). LAI at FL was based on litterfall and SLA data from similar nearby stands (Clark et al., 1999; Gholz et al., 1991).

Biomass of trees was estimated using site-specific allometric biomass relationships based on diameter at breast height (dbh), and tree height in some cases (e.g., ME), and carbon content was assumed to be 50% of biomass. Aboveground wood productivity was estimated from change in biomass and wood increment using dendrometer bands or wood cores. Foliage productivity was either estimated from annual litterfall, assuming steady-state conditions, or from foliage mass and fraction of new foliage. For example, wood production at ME was estimated from wood cores (1-year growth) and the difference between previous and current biomass calculated from site-specific allometric equations, and foliage biomass was estimated from the product of leaf mass per unit area (LMA) and LAI. Foliage productivity was estimated from fractional increase in foliage mass, and understory biomass and productivity was estimated from site-specific allometric relationships with shrub dimensions. Belowground production was estimated from belowground carbon allocation and root respiration. Belowground C allocation was estimated from annual soil surface  $\text{CO}_2$  flux minus litterfall carbon (Law et al., 2001c). At FL, carbon in components was estimated using allometric biomass relationships based on dbh for trees (Gholz et al., 1991) and plant dimensions for understory species, with organic matter assumed to be 50% carbon. Carbon accumulation in forest floor litter was estimated from litterfall measurements, assuming 15% mass loss per year (Gholz et al., 1985). Ratios of productivity and biomass estimates from different plant tissues were used to parameterize the allocation algorithms in Biome-BGC (Thornton, 1998; White et al., 2000).

## 2.3. Flux measurements

Automated measurements of  $\text{CO}_2$ , water vapor and sensible heat fluxes have been made over these forests since about 1996, as part of the AmeriFlux network and the global network, FLUXNET. The tower measurements provide estimates of net ecosystem exchange (NEE) of  $\text{CO}_2$  between vegetated surfaces and the atmosphere, with contributions from a region extending several kilometers. Although different

systems were used (open and closed path infrared gas analyzers, ATI sonics, CSAT3 sonics, GILL sonics), a calibration system was transported among sites to identify and resolve instrument or data analysis problems. Flux systems consisted of three-axis sonic anemometers that measured wind speed and virtual temperature, infrared gas analyzers that measured concentrations of water vapor and CO<sub>2</sub>, and a suite of software for real-time and post-processing analysis. Fluxes were averaged half-hourly, and the records in the database were evaluated for data quality. Data were quality checked and gaps were filled using standardized methods (Falge et al., 2002; Law et al., 2002).

## 2.4. Modeling

### 2.4.1. Model background

We used the Biome-BGC model (Thornton, 1998; Kimball et al., 1997; White et al., 2000) to simulate fluxes and storage of water, carbon, and nitrogen at each measurement site. The current version of Biome-BGC (version 4.1.1) is designed explicitly for the purpose of studying the influences of climate, disturbance and management history, atmospheric chemistry, and plant ecophysiological characteristics on the terrestrial components of the carbon, nitrogen and water cycles. Fig. 2 is a highly summarized depiction of the fluxes and state variables for carbon and nitrogen in Biome-BGC. Key model processes are described in Appendix A.

Daily surface weather data are the fundamental drivers for Biome-BGC. Given a record of daily weather, a description of the site vegetation ecophysiology, and some simple site physical characteristics, the model estimates the daily fluxes of carbon, nitrogen, and water between the atmosphere, plant state variables, and litter and soil state variables. Unlike earlier models in the BGC family (e.g., Forest-BGC, Running and Coughlan, 1988), Biome-BGC is not constrained by observed LAI. Instead, LAI is predicted as a function of the amount of leaf carbon, one of multiple vegetation state variables that are updated every day according to the estimated fluxes. The vegetation type, as defined by a set of ecophysiological characteristics, is assigned by the user and does not change over time. The state of the assigned vegetation type is fully prognostic: the model simulates changes in structure over time as interacting functions

of disturbance history, the meteorological drivers, and the constant ecophysiological characteristics of the vegetation type. The model does not currently predict interactions between different vegetation types at the same site, but simulations with multiple non-interacting types are possible (see discussion of spatial ensembling in Law et al., 2001c).

### 2.4.2. Daily surface weather inputs

In order to facilitate comparisons between sites, the daily surface weather data used in all the simulations presented here are drawn from a single database, gridded at 1 km resolution over the conterminous US, referred to as the Daymet database (Thornton et al., 1997, 2000; Thornton and Running, 1999). Using geographic coordinates for each site, the daily data for temperature, precipitation, radiation, and humidity were extracted for the nearest 1 km Daymet gridcell. The Daymet database currently covers the period of record from 1980 to 1997, and this 18-year period was extracted for each site. This 18-year record was repeated as necessary to create meteorological records for model runs of longer duration. A summary of the Daymet daily surface weather data at each site is given in Table 1.

### 2.4.3. Ecophysiological characteristics

Biome-BGC requires a static description of the ecophysiological characteristics of the vegetation at a simulation site. Although evergreen needleleaf vegetation dominates at each site in this study, the ecophysiological characteristics of the evergreen trees vary considerably between sites. There are also some sites with significant within-site variations due to evergreen species mixtures. Leaf longevity ranges between sites from 2 years for slash pine to 5 or more years for spruce and Douglas-fir. Other important variations include parameters controlling the allocation of new production to leaves, wood and fine roots.

Parameters for the dominant evergreen conifer species were used to characterize the ecophysiology at each site, using data gathered on-site when available, and species-specific values from a recent literature synthesis otherwise (White et al., 2000). The ecophysiological parameters for each site are listed in Appendix B together with a brief description of the parameters and their units. The sensitivity of the model to variation in these parameters has been

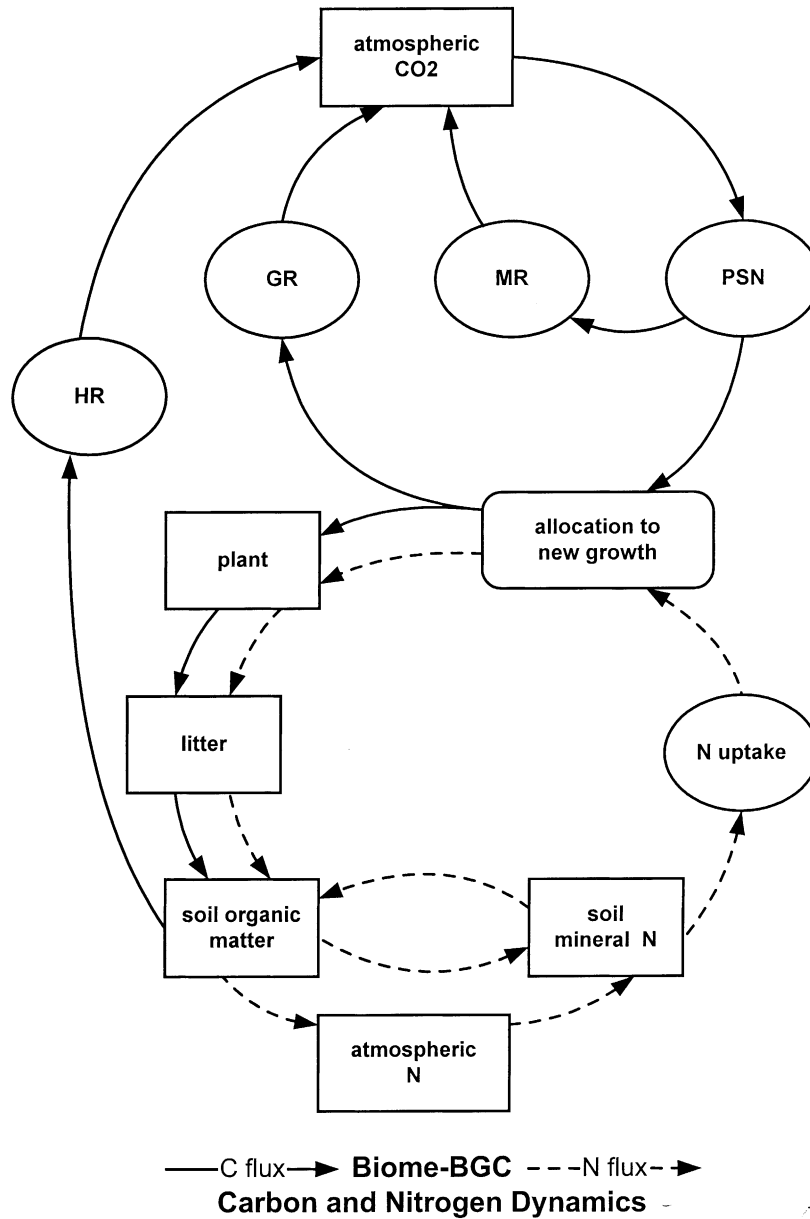


Fig. 2. Simplified schematic of the fluxes (arrows) and state variables (square boxes) for the carbon and nitrogen components of the Biome-BGC model. Some processes are shown as rounded boxes: photosynthesis (PSN), maintenance respiration (MR), growth respiration (GR), heterotrophic respiration (HR), plant N uptake, and allocation of C and N to new plant growth. Solid lines indicate C fluxes, dashed lines indicate N fluxes. The plant, litter and SOM boxes shown here consist of multiple model state variables. Detailed model process descriptions are in [Appendix A](#).

described for a range of plant functional types (White et al., 2000). The model sensitivity to variation in some of the allocation parameters was recently described for simulations at ME (Law et al., 2001c).

#### 2.4.4. Modeling analysis overview

The analysis consisted of model initialization followed by a series of simulations designed to replicate as closely as possible the known disturbance history of each site. The results of the site-specific disturbance history simulations were compared with recent eddy covariance and biometric measurements at the sites. The timing and magnitude of fluxes during recovery from disturbance were related to environmental factors, disturbance history, and the timing of disturbance with respect to historical changes in CO<sub>2</sub> and N<sub>dep</sub>.

The foundation for model simulations at each site is a precursor (or spinup) run used to bring the model state variables into steady-state with respect to the site climate and the specified vegetation ecophysiology. At this steady-state there is still variation due to interannual variability in the weather record, but the long-term mean fluxes are stationary, and the long-term mean NEE is 0 (NEE is taken here as positive for a net sink, negative for a net source to the atmosphere). The main purpose of the spinup run is to bring soil organic matter (SOM) into a dynamic equilibrium with the specified climate and vegetation type. Since SOM accumulates as a result of litter decomposition, and since the mineralization of SOM provides most of the nitrogen required for new plant growth, there are strong feedbacks between the development of plant and soil pools of carbon and nitrogen.

The spinup run begins with no SOM and a very small initial vegetation component. The rate of accumulation of SOM over time during the spinup is highly dependent on the rate of addition of nitrogen (wet and dry deposition plus symbiotic and asymbiotic fixation, Appendix B). At typical deposition and fixation rates this process can take tens of thousands of simulation years. To accelerate the spinup process a mechanism is employed to periodically increase the addition of mineral nitrogen during the early part of the spinup run, using the rates of change in the SOM pools to assess the proximity to steady-state. This reduces the typical spinup time by about a factor of 10 (average ~2000 simulation years), and produces the

same steady-state conditions obtained without accelerated nitrogen additions.

Using the spinup endpoint as an initial condition, we constructed simulation sequences based on the history of disturbance and management practices at each site. This allowed us to compare the predicted states and fluxes at a given site with recent observations. Simulation ensembling was used to remove the effects of interannual variation, leaving a signal that could be attributed entirely to the disturbance recovery response. Ensemble results provided both mean values and standard deviations due to interannual climate variability for the fluxes and state variables at the current stand ages.

#### 2.4.5. Ensembling methods

Because surface weather parameters vary from year to year, the temporal effects of a particular disturbance will be expressed somewhat differently at the same site depending on the timing of the disturbance relative to interannual climate variations. This variability obscures the temporal details of the disturbance recovery response. We removed the effects of interannual climate variability from the recovery response time series by performing an ensemble of simulations initiating from each disturbance event, with one ensemble member for each year of meteorological data in the input dataset. In the case of the 18-year record of the Daymet dataset, each of the disturbance recovery responses was calculated as the average of 18 independent model simulations, with the disturbance initiated at the beginning of a different year in each ensemble member.

#### 2.4.6. Simulation of disturbance

Four different disturbance types are relevant to this study: wildfire, harvest, slashburning, and replanting (we use “disturbance” here to indicate both natural disturbances and management actions). We have implemented a simple definition for the effects on model state variables of each disturbance type. These definitions allow for different disturbance levels within a type (Appendix C).

We used the available disturbance history information from each site (Table 2) to construct a time series of disturbances, management practices, and changes in atmospheric CO<sub>2</sub> concentration and N<sub>dep</sub>. Because steady-state conditions from the spinup runs assume a constant atmospheric CO<sub>2</sub> concentration of 280 ppmv

(characteristic of conditions in 1795), the disturbance history simulations at each site were at least 205 years long to include the time course of changes in CO<sub>2</sub> from 1795 to 2000. Changes in CO<sub>2</sub> concentration over time followed the IS92a scenario (Enting et al., 1994). Using observations of current N<sub>dep</sub> from the closest NADP measurement station (NADP, 2000), we simulated the time course of N<sub>dep</sub> assuming that it varied from its pre-industrial levels to current levels at each site in concert with the rising concentration of CO<sub>2</sub> (Table 1). In some cases the disturbance history at a site extends to periods before 1795, in which case the period between the first known disturbance event and 1795 is simulated with constant CO<sub>2</sub> and N<sub>dep</sub>.

The final year of the site history simulations consisted of 18 ensemble members, one for each of the years in the daily meteorology records. These members were used to find averages and interannual standard deviations for various flux and storage components, which were compared with the available observations on both an annual and a monthly basis.

To evaluate the interactions between episodic disturbance and changing atmospheric chemistry we performed a parallel series of model simulations keeping CO<sub>2</sub> and N<sub>dep</sub> constant at the pre-industrial levels. The difference between ensemble averages for these two sets of simulations was taken as the contribution of a changing atmosphere to the disturbance recovery dynamics at each site.

### 3. Results and discussion

To provide a context for discussion, we first report the results of the historical simulations at each site. We then describe the comparison of ensemble model results from the final simulation year with observations, using monthly and annual summaries. Finally, we present the results from a series of model sensitivity tests, including an analysis of the interaction effects between disturbance history and changes in atmospheric CO<sub>2</sub> and N<sub>dep</sub>.

#### 3.1. Predicted historical patterns of disturbance recovery

Fig. 3 shows the ensemble average and interannual standard deviation for the modeled history of NEE

response to disturbance at each site. All site simulations extended at least as far back as 1795, but only the period of documented disturbance history at each site is shown. A similar pattern is evident in the model results for all sites: a net carbon source beginning immediately after disturbance and diminishing with time, followed by a longer period during which the site is a net carbon sink.

The simulated peak annual carbon sources occur within 2 years of a stand-replacing disturbance at all sites, and range from 300 to 850 g C m<sup>-2</sup> per year (f1, Table 3). There are clear differences between sites in the time after disturbance before the site switches from a net source to a net sink of carbon (t1, Table 3). The longest such periods followed stand-replacing fires at ME and WR, where the sites were continuous annual sources of carbon for 14 and 16 years, respectively. The shortest simulated recovery periods (4–6 years) followed intensively managed harvests at BL, DU and FL. Simulated recovery periods were of intermediate duration following simple harvests at HL and NR. The total source during the continuous source period (s1, Table 3) was between 1400 and 3100 g C for all sites except WR, which lost almost 8500 g C before switching to a net annual sink. These total carbon sources do not include the carbon lost from site as a direct consequence of disturbance (combustion or harvest removals). For example, historical patterns of tree utilization in the Pacific northwest suggest that approximately 95% of carbon stored in live tree boles can be removed by harvest, and 50% of this is lost to the atmosphere during the first year (Harmon et al., 1996). Other studies suggest that 10–25% of wood can be lost to combustion.

Peak simulated carbon sinks occurred within 2–7 years after the site first became a net sink following disturbance, with peak sink strengths ranging from 123 g C m<sup>-2</sup> per year for ME to more than 500 g C m<sup>-2</sup> per year at DU and WR. The difference between simulated peak and current sink strengths are directly related to the time since disturbance: the recently harvested sites (BL, DU and FL) are very near their peak sink strengths in net uptake per year, while the old sites (ME and WR) are currently very small annual net sinks. The intermediate aged sites (HL and NR) have simulated current sink strength of less than half their peak values.

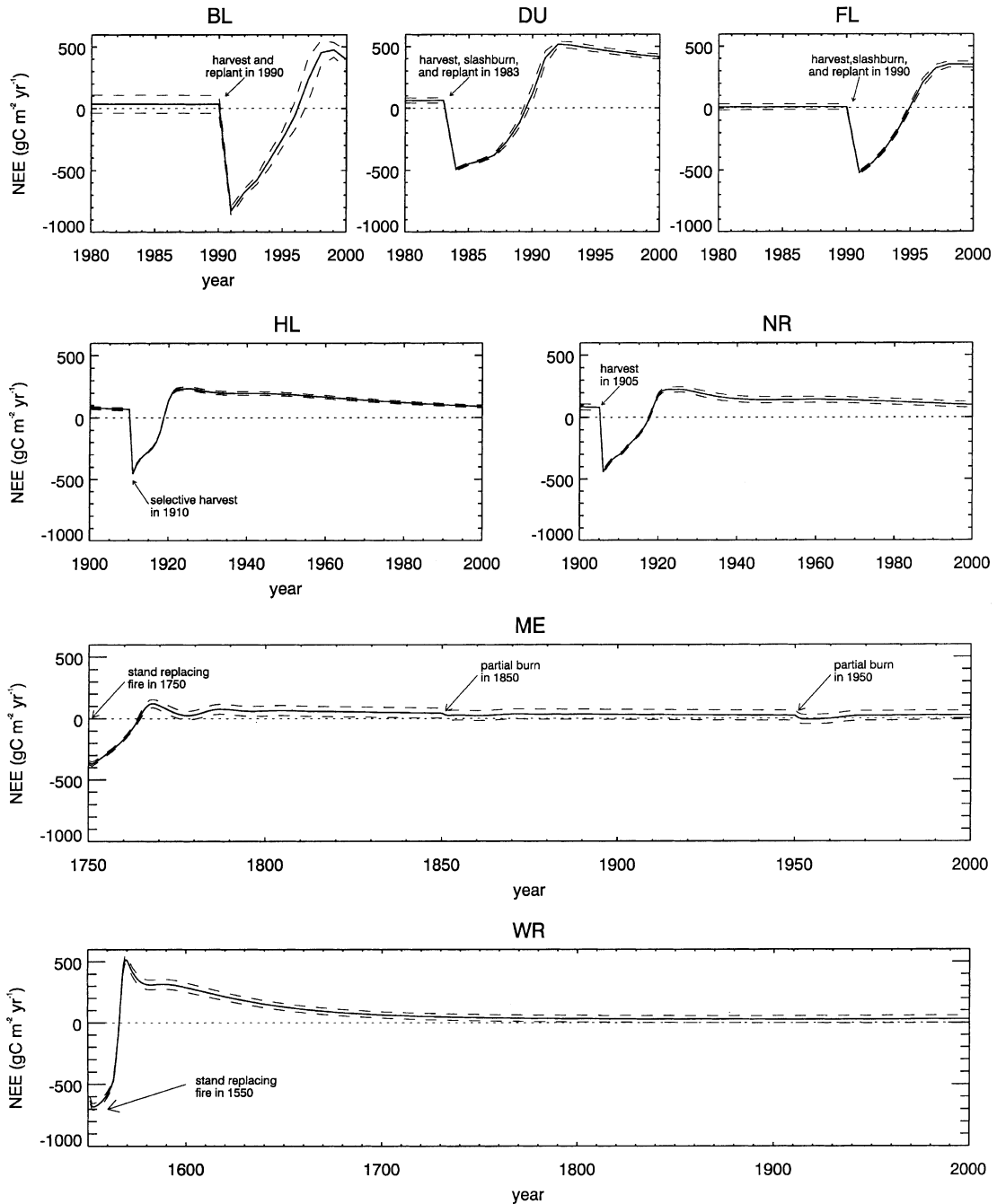


Fig. 3. Time series of model NEE for each study site using the site disturbance histories (Table 2) and the disturbance mechanisms defined in Appendix C. The time series for each site is shown from at least the time of the most recent major disturbance. Arrows indicate the time and type of disturbance. Because of the very different lengths of time since major disturbance the time axes are scaled differently. Negative NEE is a source to the atmosphere, positive NEE is a sink. Shown are the mean of the 18 ensemble runs at each site (solid line) and the interannual standard deviations from the ensemble (long dashed lines). The neutral NEE line is included (short dashed line).

Table 3  
NEE dynamics during disturbance recovery<sup>a</sup>

Site	Most recent disturbance type and date	t1 (years) <sup>b</sup>	f1 (g C m <sup>-2</sup> per year) <sup>c</sup>	s1 (g C m <sup>-2</sup> ) <sup>d</sup>	t2 (years) <sup>e</sup>	f2 (g C m <sup>-2</sup> per year) <sup>f</sup>	NEE <sub>cur</sub> (g C m <sup>-2</sup> per year) <sup>g</sup>	Δs (g C m <sup>-2</sup> ) <sup>h</sup>
BL	Harvest and replant (1990)	6 (–1)	826 (–7)	2796 (–189)	8 (–1)	474 (+91)	393 (+10)	(+1098)
DU	Harvest, slashburn, replant (1983)	6 (–1)	492 (+21)	2125 (–133)	8 (–3)	518 (+63)	416 (+37)	(+2424)
FL	Harvest, slashburn, replant (1990)	4 (–3)	522 (+2)	1486 (–686)	8 (–1)	351 (+160)	349 (+158)	(+2498)
HL	Harvest (1910)	8 (0)	455 (+1)	2272 (+10)	14 (–1)	238 (+13)	89 (+10)	(+700)
ME	Stand-replacing fire (1750)	14 (0)	371 (0)	3046 (0)	17 (0)	123 (0)	25 (+2)	(+156)
NR	Harvest (1905)	12 (–1)	441 (+1)	3007 (–73)	19 (–1)	227 (+11)	100 (+12)	(+853)
WR	Stand-replacing fire (1550)	16 (0)	681 (0)	8498 (0)	18 (0)	517 (0)	29 (+3)	(+219)

<sup>a</sup> Model results during vegetation recovery following the most recent large disturbance at each site. Simulations include the observed increases over time in CO<sub>2</sub> and N<sub>dep</sub>. Values in parentheses are the estimated effects of changing CO<sub>2</sub> and N<sub>dep</sub> during disturbance recovery on each parameter.

<sup>b</sup> Number of years during which the site was a continuous net carbon source following disturbance.

<sup>c</sup> Peak annual carbon source following disturbance.

<sup>d</sup> Total carbon source from time of disturbance to t1.

<sup>e</sup> Time from disturbance to peak annual net carbon sink.

<sup>f</sup> Peak annual carbon sink following disturbance.

<sup>g</sup> Current NEE (year 2000, positive for net sink).

<sup>h</sup> Total change in ecosystem carbon content since 1796 due to increasing CO<sub>2</sub> and increasing N<sub>dep</sub>.

Stands at ME and WR have multiple age classes characteristic of old-growth forest structure. Stand age structure for ME suggests at least two partial fire events over the past 250 years, each affecting about 25% of the stand area. Local knowledge suggests that the 50-year-old age class was the first successful cohort during fire suppression over the past 100 years, likely from several favorable years of precipitation that allowed the seedlings to become established in this region where summer drought typically occurs (Rod Bonacker, pers. comm.). This dynamic was not taken into account in the simulations, but when we assumed that two partial fire events took place, they had little effect on the long-term trajectory of predicted diminishing sink strength at the site. Simulated peak sink strength of over 100 g C m<sup>-2</sup> per year lasted several decades, with the current simulated sink at 25 g C m<sup>-2</sup> per year. There is only strong evidence of a single fire disturbance 400–500 years ago at WR, and although the sink strength was quite high for several decades and greater than 100 g C m<sup>-2</sup> per year for almost a century, the predicted sink strength has been close to 30 g C m<sup>-2</sup> per year for the past 200 years.

### 3.2. Comparison of model results with observations

#### 3.2.1. LAI

Observed values for LAI in either one-sided or projected units are given in Table 4. Model estimates of projected LAI at current stand conditions are shown for each site in Table 5, and are plotted against observed LAI in Fig. 4. Agreement is generally very good, but the model estimate of LAI at HL is low by about 20%. The model accurately represents the two sites that bracket the range of observed LAI in this study (WR at 8.6 and FL at 2.0). It is interesting that in spite of the very dramatic difference in LAI, these sites are predicted to have the highest NPP and GEP (Table 6). In fact, FL with the lowest LAI has both NPP and GEP predicted to be higher than WR. Leaf longevity is a very important factor in these predictions. It is estimated as 2 years for slash pine at FL, and 6 years for Douglas-fir at WR (observed range at WR is 4–8 years). These results may help to explain the weakness of the relationship between LAI and GEP found by Law et al. (2002). These two sites are also predicted to have the highest evapotranspiration (ET).

Table 4  
Observed LAI and sources<sup>a</sup>

Site	Observed LAI and units	Source
BL	4.5 (1s)	Xu et al. (2001)
DU	4.15 (pr) mean of annual min. (2.9) and annual max. (5.4)	D. Ellsworth (pers. comm.)
FL	2.05 (pr) sum of pine (1.6) and evergreen broadleaf (0.45)	H. Gholz (pers. comm.)
HL	5.5 (pr)	Hollinger et al. (1999)
ME	2.1 (1s)	Law et al. (2001c)
NR	3.99 ± 0.39 (pr)	J. Sparks (pers. comm.)
WR	8.6 (1s)	J. Chen (pers. comm.)

<sup>a</sup> Units are either projected (pr) or one-sided (1s).

If the modeled contributions to ET from the evaporation of canopy intercepted water are ignored, FL has the highest rate and WR the third highest.

### 3.2.2. Monthly water and carbon fluxes

Ensemble members for the final year of simulation at each site were combined to produce average monthly values and interannual standard deviations for these monthly values for the main components of the carbon budget, and for ET. Model carbon budget components include NEE, total ecosystem respiration ( $R_e$ ), and gross ecosystem production (GEP).

ET comparisons were performed using two different summaries of the model ET, one having all the components of evaporation and transpiration (ET<sub>m</sub>) and the other including all components except evaporation of intercepted rainwater from the canopy (ET<sup>\*</sup><sub>m</sub>). This is done because there is a suspected flux underestimation bias in the measurements when the sonic anemometers are wet, and we assumed that the period of instrument drying would correspond roughly

to the period of evaporation from a wet canopy. The values of ET<sub>m</sub> (Fig. 5a) for BL and WR show very large overpredictions in the winter months, when most of the wet days occur at these sites. The seasonal biases at these sites are greatly reduced when comparing ET<sup>\*</sup><sub>m</sub> with the monthly observations (Fig. 5b), although for both comparisons the model underestimates summer ET at BL, and overestimates summer and fall ET at WR. Stand and leaf level measurements at WR show severe water stress in the summer and early fall, which is not seen in the model ensemble mean. The GILL sonic anemometers used at WR are less prone than CSAT3 sonics to measurement biases when wet, and so the model contribution to ET from canopy evaporation may be too large. Comparisons at DU show an overestimation bias in the winter months with ET<sub>m</sub>, and an underestimation bias in the summer months with ET<sup>\*</sup><sub>m</sub>. Comparisons at NR show an underestimation bias in late winter and an overestimation bias in mid-summer, neither of which are very sensitive to the choice of ET<sub>m</sub> or ET<sup>\*</sup><sub>m</sub>. Use of ET<sup>\*</sup><sub>m</sub>

Table 5  
Model estimates of current (2000) site carbon storage<sup>a</sup>

Site	LAI	Leaf C	Veg C	AG veg C	BG veg C	Litter C	CWD C	SOM C	Total C
BL	4.12 (0.36)	535 (47)	2042 (230)	1419 (171)	624 (59)	312 (89)	1046 (25)	3667 (50)	7068 (384)
DU	4.00 (0.08)	377 (8)	5434 (61)	4923 (55)	511 (6)	386 (14)	457 (3)	1720 (8)	7996 (60)
FL	2.06 (0.03)	361 (5)	2658 (49)	1958 (37)	700 (12)	116 (7)	633 (5)	1834 (11)	5241 (65)
HL	4.30 (0.03)	430 (3)	15189 (30)	12371 (24)	2818 (7)	493 (4)	1580 (3)	2697 (4)	19959 (34)
ME	2.35 (0.08)	305 (10)	8540 (50)	6859 (25)	1681 (27)	576 (40)	961 (3)	3918 (17)	13995 (43)
NR	3.74 (0.05)	374 (5)	12386 (23)	10072 (16)	2314 (7)	862 (23)	2489 (8)	4708 (6)	20445 (40)
WR	8.73 (0.03)	873 (3)	34196 (48)	30373 (42)	3823 (7)	715 (11)	3955 (13)	5482 (8)	44348 (68)

<sup>a</sup> Each state variable is shown as a mean value for current stand age, with the estimated standard deviation due to interannual climate variability in parentheses. LAI is on a projected area basis and is based on the annual mean. Units are in g C m<sup>-2</sup>, for the other variables: total vegetation carbon (veg C), aboveground vegetation carbon (AG veg C), belowground vegetation carbon (BG veg C), litter carbon, excluding CWD (litter C), coarse woody debris carbon (CWD C), soil organic matter carbon (SOM C) and total ecosystem carbon (total C).

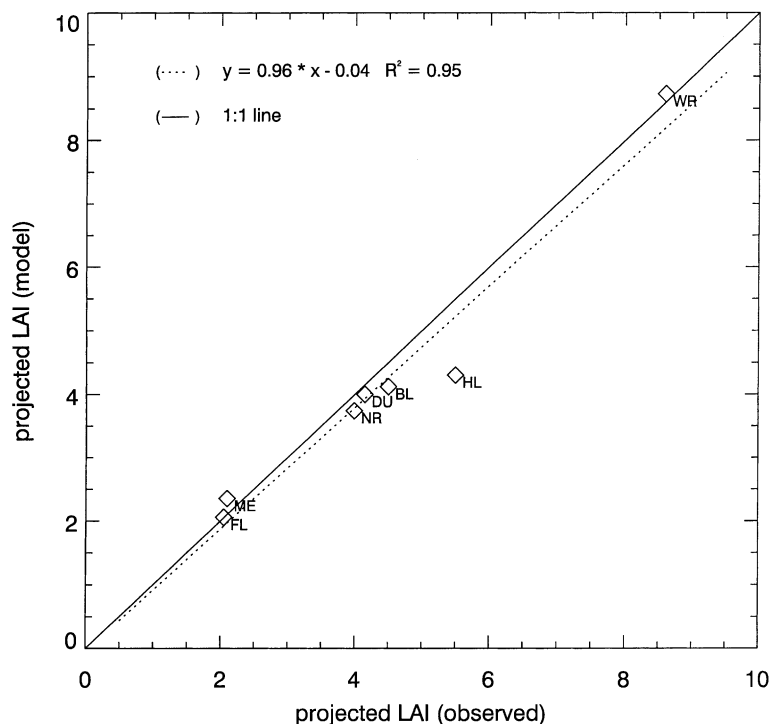


Fig. 4. Predicted vs. observed annual average LAI. All model estimates are in projected area units, and all observed values use either projected or one-sided units (see Table 4).

removes a moderate overestimation bias for summer, fall and early winter at HL. Monthly ET comparisons show low biases at ME under both ET<sub>m</sub> and ET<sup>\*</sup><sub>m</sub>.

At FL, ET<sub>m</sub> is underestimated by as much as 25% during the summer months, with even stronger sum-

mer biases for ET<sup>\*</sup><sub>m</sub>. The fact that LAI is simulated accurately at both BL, DU and FL, while summer ET is underestimated (for the ET<sup>\*</sup><sub>m</sub> comparisons), suggests that the maximum value of stomatal conductance may have been set too low in the ecophysiological

Table 6

Model estimates of current (circa 2000) annual carbon and water fluxes<sup>a</sup>

Site	NEEm	R <sub>e</sub> m	GEPm	NPPm	ANPPm	BNPPm	FRNPPm	ETm	ET <sup>*</sup> <sub>m</sub>
BL	393 (78)	1432 (72)	1825 (62)	712 (71)	486 (30)	267 (17)	243 (15)	686 (77)	553 (30)
DU	415 (21)	1219 (39)	1635 (50)	714 (21)	642 (15)	74 (2)	29 (1)	586 (25)	471 (15)
FL	349 (25)	1869 (47)	2236 (58)	786 (26)	542 (12)	236 (5)	140 (3)	715 (25)	650 (20)
HL	89 (11)	1149 (32)	1238 (34)	401 (14)	272 (5)	127 (2)	91 (2)	425 (25)	335 (10)
ME	25 (36)	1094 (32)	1119 (49)	377 (32)	162 (9)	214 (12)	202 (12)	443 (28)	381 (17)
NR	100 (23)	801 (21)	901 (34)	351 (16)	238 (7)	111 (3)	79 (2)	492 (25)	463 (28)
WR	29 (30)	2151 (61)	2179 (49)	659 (24)	468 (9)	187 (4)	156 (3)	977 (92)	537 (15)

<sup>a</sup> Each flux is given as a mean value for the current stand age and disturbance history, with a standard deviation from interannual climate variability in parentheses. Units are in g C m<sup>-2</sup> per year for net ecosystem exchange (NEEm, positive for a sink), total ecosystem respiration (R<sub>e</sub>m), gross ecosystem production (GEPm), net primary production (NPPm), aboveground net primary production (ANPPm), belowground net primary production (BNPPm), fine root net primary production (FRNPPm). Units are in mm per year for total evapotranspiration (ETm) and ET excluding the evaporation of water intercepted on the canopy during rain events (ET<sup>\*</sup><sub>m</sub>).

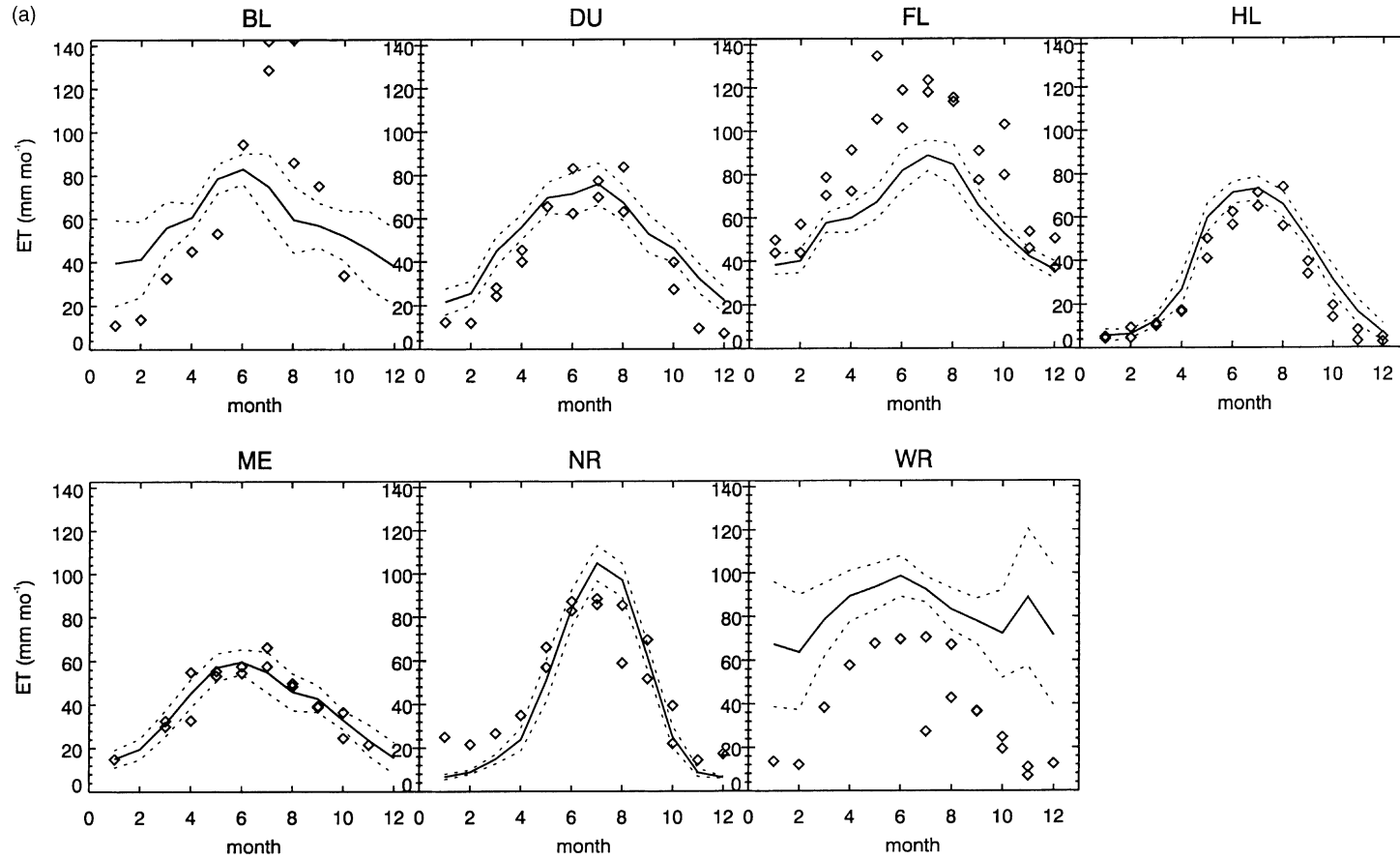


Fig. 5. Seasonal cycle of model and observed monthly ET. Model results shown for both total ET (a) and for all components of ET except the evaporation of canopy intercepted water (b). Solid line shows the ensemble mean seasonal cycle for the final year of simulation (comparable to 2000 A.D. on the basis of time since disturbance). Dashed lines show the interannual standard deviations from ensemble mean. Symbols show the observations for each month, with multiple symbols for a single month when there are multiple years of observation.

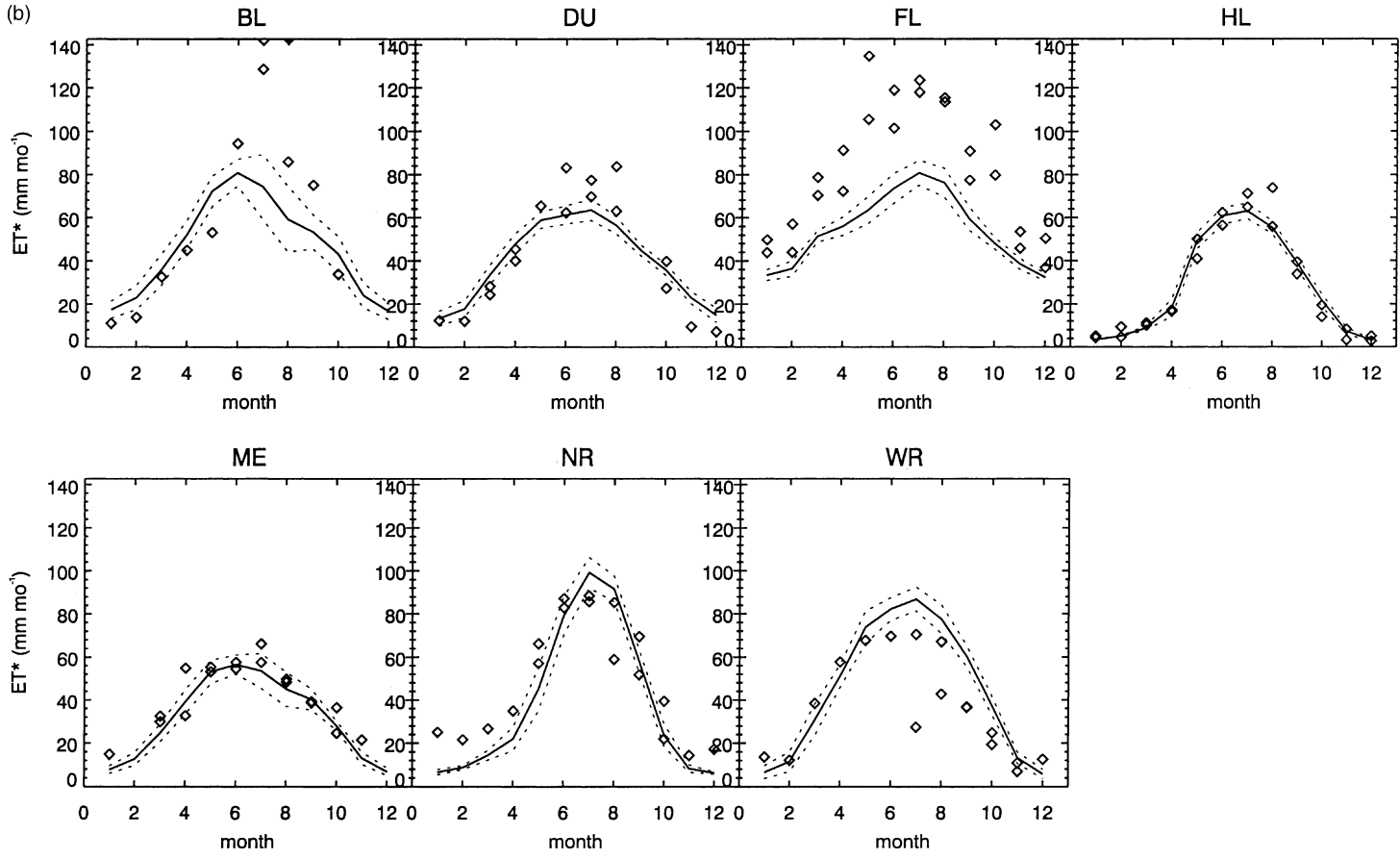


Fig. 5. (Continued).

parameterizations for these sites (Appendix B). The fact that these are the youngest sites, and all about the same age, suggests that there may be an important age-dependence for maximum stomatal conductance that has not been included in the model.

Scatter plots of the monthly mean ensemble values of  $ET_m$  and  $ET^*_m$  against averaged observations for each month show the general improvement in comparisons using  $ET^*_m$  (Fig. 6a and b). Since the LAI comparisons are very good, it seems reasonable to infer from the improved fit using  $ET^*_m$  that the observations at some sites and in some seasons are in fact biased by underestimating evaporation during periods when the canopy is wet. It is also possible that compensating model errors produce LAI close to observations while overestimating the evaporation of canopy intercepted water.

Monthly comparisons for NEE show model underestimation biases for mid-summer sink strength at all sites (Fig. 7). There is an overestimation bias of sink strength in the winter at BL, DU and NR, and an underestimation bias in winter at ME. Model and observed NEE are in general agreement for the period September–April at HL, and July–December at NR and WR. Monthly averages of the observations at each site are compared to the simulation ensemble mean for each month (Fig. 8), illustrating the poor overall correlation.

The consistent underestimation of sink strength during the summer indicates that the model warm season respiration is too high, or model GEP is too low, or model estimates are correct and the summer fluxes observations have a net sink bias, or some combination of these causes. To begin to address this range of possibilities, monthly estimates of total ecosystem respiration ( $R_e$ ) derived from flux data (Falge et al., 2002) are compared to model estimates of  $R_e$  (Fig. 9: note that not all sites report  $R_e$ ).

Biome-BGC estimates of  $R_e$  are based on a sum of the three separate components: two autotrophic components (maintenance and growth respiration) and heterotrophic respiration from the decomposition of litter and SOM (see Appendix A for process descriptions). At BL, DU, NR and WR, the flux-based estimates of  $R_e$  are derived from relationships between night time fluxes and air temperature, for periods when wind speed is above a critical level (Falge et al., 2002, M. Falk, pers. comm.). At ME, estimates

of  $R_e$  are based on direct soil chamber, bole, and leaf chamber measurements made in all seasons and scaled for air temperature (Law et al., 2001c).

At BL and DU there are clear overestimates of summer  $R_e$  from the model compared to estimates derived from the flux data, while at WR the model  $R_e$  is higher than the flux-derived estimates in all months. At most of these sites the seasonal shape of the respiration curve is similar between model and flux-based estimates, but at BL the flux-based estimate of  $R_e$  declines in the mid-summer, when the Biome-BGC estimate is increasing with rising temperature. At FL, ME and NR, modeled and observed  $R_e$  are in reasonable agreement through the spring summer and fall, with model overestimates of  $R_e$  during the winter at ME and underestimates during the winter at FL. Monthly averages of the observations and the monthly mean of the ensemble simulations are shown as a scatter plot in Fig. 10.

The use of chamber measurements makes the comparison at ME a useful point of reference for the  $R_e$  comparisons at the other sites. The sum of model heterotrophic and autotrophic respiration for the period April–November is in very good agreement with observations at ME that are independent of potential measurement biases associated with the eddy covariance methods. Law et al. (1999) showed that under weak nocturnal wind conditions,  $R_e$  from eddy covariance methods was 23% lower than ecosystem respiration calculated from the chamber measurements. The flux screening procedures (Falge et al., 2002) were expected to remove data under these conditions.

The seasonal cycle of modeled and flux-based GEP is shown in Fig. 11. It is important to note that the flux-based values for GEP are constrained as the difference between measured NEE and flux-based  $R_e$  (or chamber-based  $R_e$  in the case of ME). The most significant biases are at BL and WR, where the model consistently overestimates GEP, and at FL, where the model underestimates GEP. There are also significant overestimates during the winter at DU and NR.

In contrast to the consistent model underestimate of summer ET at the young sites (BL, DU and FL), the model overestimates summer GEP at BL, is close to summer observations at DU, and underestimates GEP through the year at FL. These bias patterns could be related to the use of a single value for the fraction of leaf nitrogen in Rubisco (see Appendix B) for all sites: additional analysis of leaf-level assimilation data for

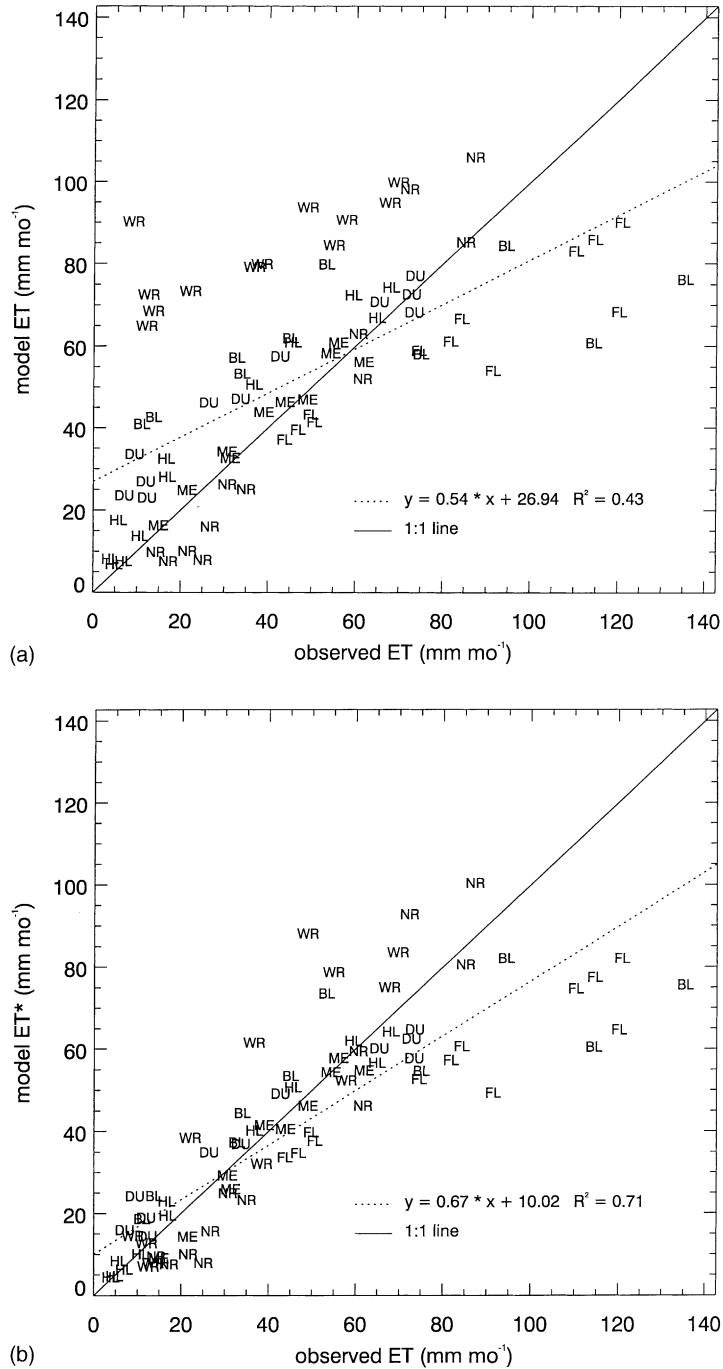


Fig. 6. Model vs. observed monthly ET, for both model total ET (a) and model ET without evaporation of canopy intercepted water (b) in the final simulation year. Symbols indicate the site, and each point represents the model ensemble mean vs. the site average of all observations for a given month.

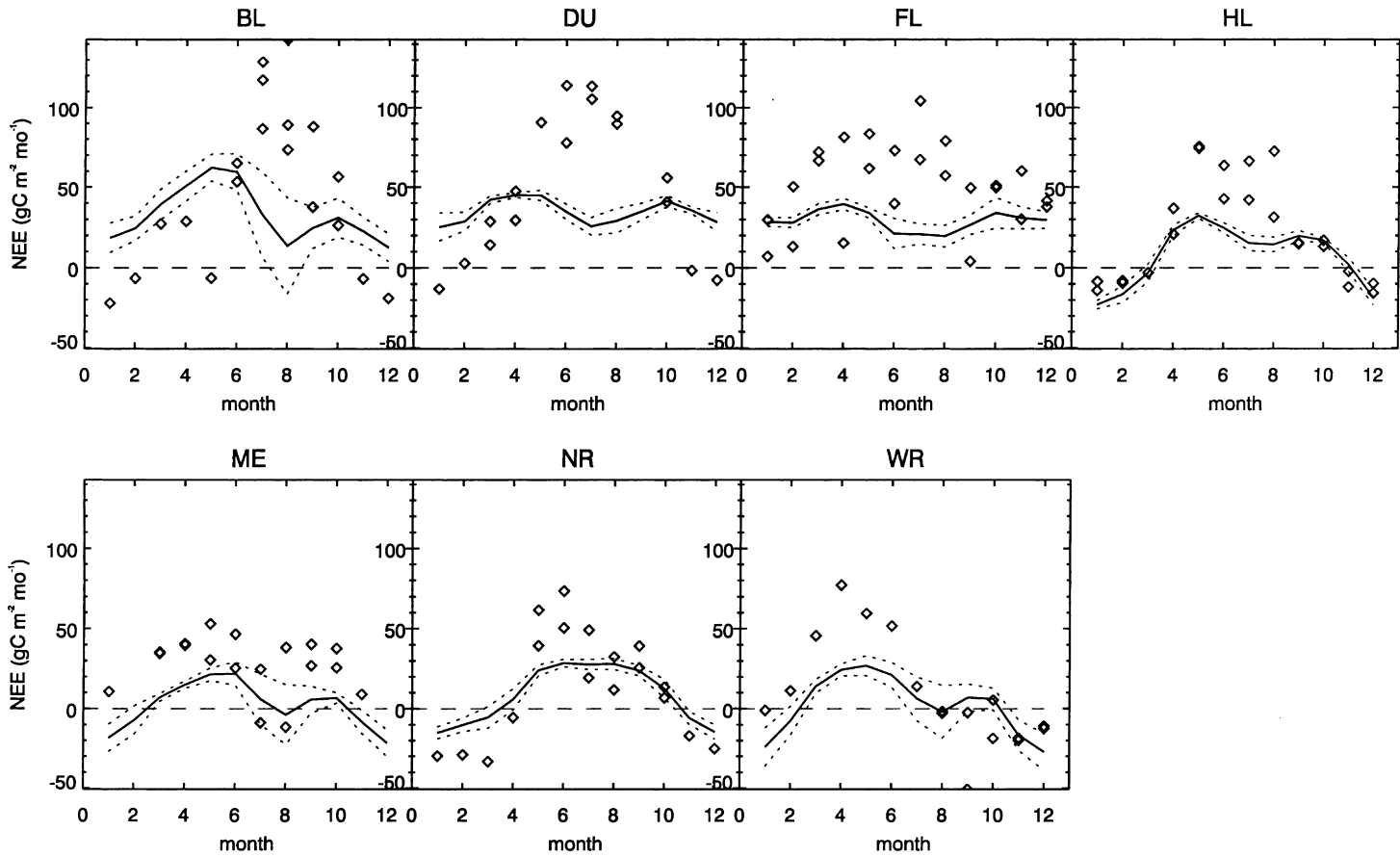


Fig. 7. Seasonal cycle of model and observed monthly NEE in the final simulation year. Lines and symbols as in Fig. 5.

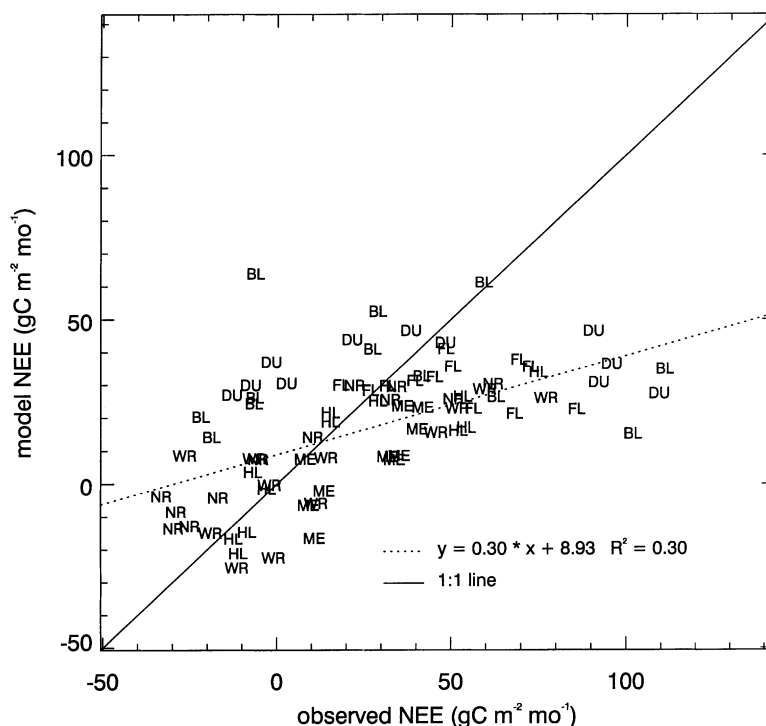


Fig. 8. Model vs. observed monthly NEE in the final simulation year. Symbols as in Fig. 6.

slash pine (FL), loblolly pine (DU), and ponderosa pine (BL) could help to address this issue (see e.g., Law et al., 2001c; White et al., 2000).

The differences between model and observed monthly carbon flux components are conveniently summarized by comparing the respective distributions with monthly average air temperature. Model NEE shows a consistent pattern of increasing sink strength as monthly average air temperature rises toward 15 °C, and decreasing sink strength for higher temperatures (Fig. 12a). Old stands approaching steady-state fluxes have smaller monthly sinks for the same temperature than young sites recovering from recent disturbance. Observed monthly NEE shows a very different overall pattern, with the highest sink strengths at temperatures over 20 °C. There is some variation in this pattern between sites, with ME and WR showing decreasing or flat observed NEE for higher temperatures, in agreement with the shape of the seasonal cycle of NEE from the model (Fig. 7).

Differences in monthly NEE can be partly explained by different temperature responses for  $R_e$  between

model and observations (Fig. 12b). Model  $R_e$  increases with temperature at every site, with larger  $R_e$  for a given temperature at sites with more biomass in the vegetation and litter. A similar pattern is apparent for some sites in the temperature dependence of observed  $R_e$ , but the increase with high temperature are not as great at most sites. At BL, measured  $R_e$  is seen to decrease at the highest monthly temperatures for that site. FL and ME have the same general pattern with temperature in the observations and model results.

The overall response of GEP to temperature is similar in the observations and model results (Fig. 12c), with the exception of a model positive bias at WR and a model negative bias at FL. The correlation of model vs. observed monthly GEP ( $R^2 = 0.66$ ) is better than for either  $R_e$  ( $R^2 = 0.52$ ) or NEE ( $R^2 = 0.30$ ).

### 3.2.3. Annual water and carbon fluxes

Different methods were available for estimating annual ET from observations. One set of annual ET observations (ET1) is available from the AmeriFlux group, based on methods described in Law et al.

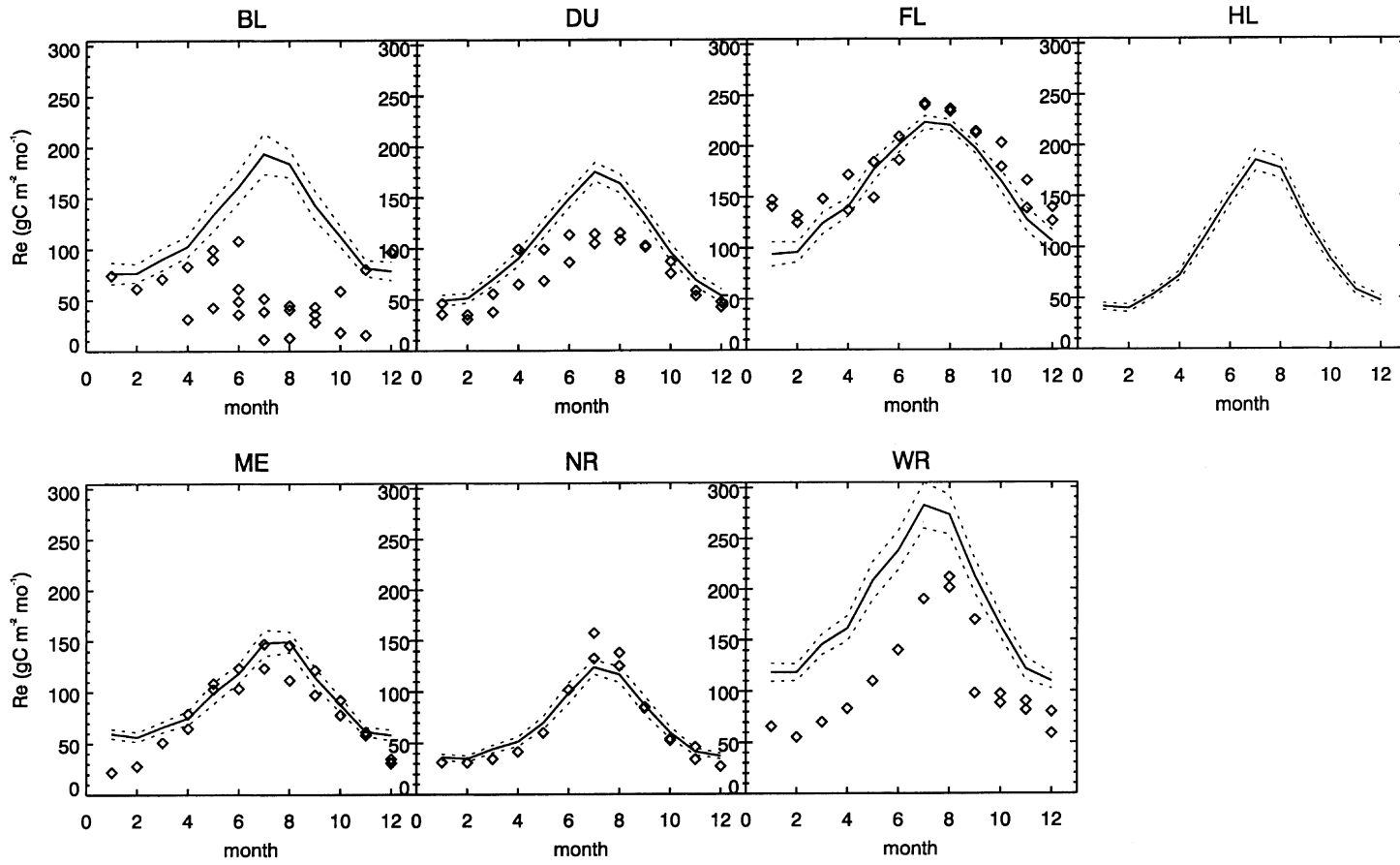


Fig. 9. Seasonal cycle of model and observed monthly  $R_e$  in the final simulation year. Lines and symbols as in Fig. 5.

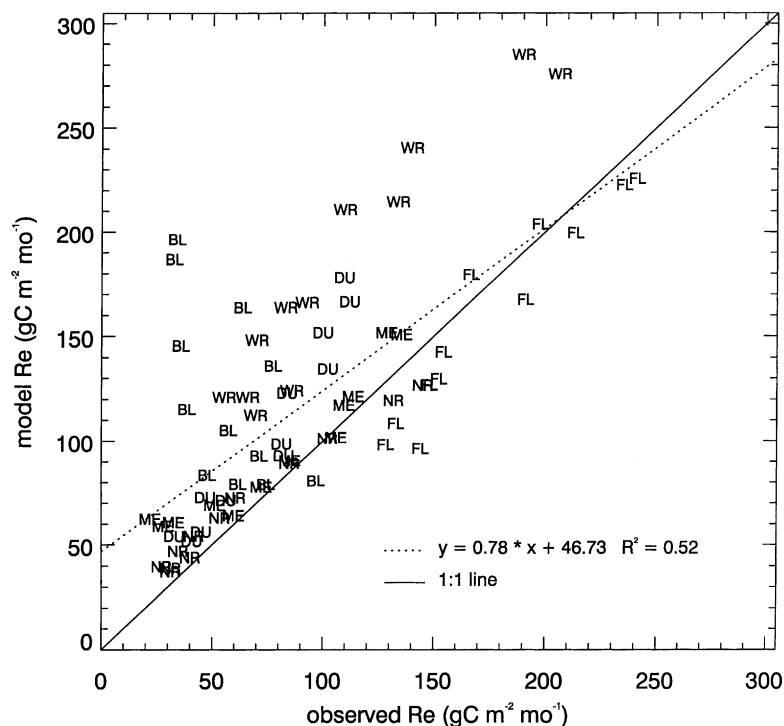


Fig. 10. Model vs. observed monthly  $R_e$  in the final simulation year. Symbols as in Fig. 6.

(2002). We generated a second set (ET2) by averaging the ET observations from Fig. 8 within months for each site, and taking the annual total of these averages. Simple linear interpolation was used to fill missing months (a total of 5 months for the seven sites). Because these first two estimates of ET differed somewhat at some sites, we generated a third set of observed values (ET3) as the average of the first two values (Table 7). Each of these sets of observed values was compared against both model estimates of ET (ET<sub>m</sub> and ET<sup>\*</sup><sub>m</sub>) (Table 8). The averaged values from the two methods of estimating annual flux-based ET (ET3) compared most favorably with the model estimates. Fig. 13 shows the results of this comparison for ET<sup>\*</sup><sub>m</sub>. The significant underestimates of ET at four sites (BL, FL, NR and ME) are not related to a consistent seasonal pattern of bias: the model underestimates of ET occur through the year at FL, in the summer at BL, and in the winter at ME and NR. The improved comparisons using ET<sup>\*</sup><sub>m</sub> (Table 8) are due mostly to the reduced error at WR. If a measurement

bias under wet-canopy conditions does exist, it may not be expressed consistently across sites.

Annual values for observed NEE are compared to model estimates, including estimates for interannual variability in both model and observations (Fig. 14). Compensating seasonal model biases at BL and NR result in relatively good annual comparisons, while the modeled annual NEE is less than that of the flux measurements at all other sites by between 160 and 230 g C m<sup>-2</sup> per year. As a percentage of the flux measurement annual net sink, the model underestimates are 30% at DU, 43% at FL, 64% at HL, 84% at WR and greater than 90% at ME.

In an earlier study, Gholz and Fisher (1982) measured the total carbon content (vegetation, litter and soil) for a chronosequence of plantation stands near the FL site. Three plots each were measured in stands aged 2, 5, 8, 14, 18 and 26 years. We used the difference in total carbon between unique pairs of plots in adjacent age classes, and a single estimate of the total carbon immediately following a typical clear-cut, to estimate

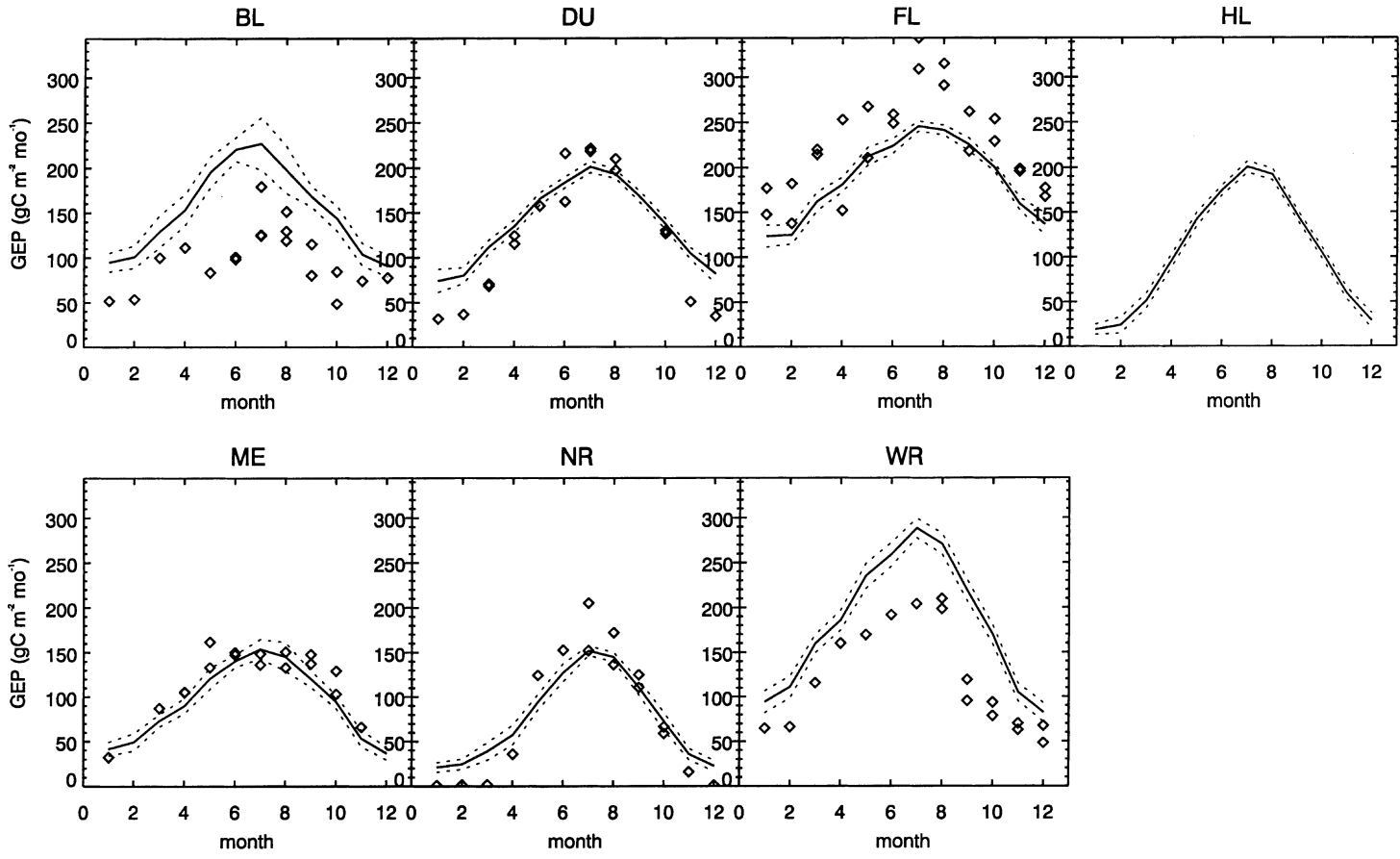


Fig. 11. Seasonal cycle of model and observed monthly GEP in the final simulation year. Lines and symbols as in Fig. 5.

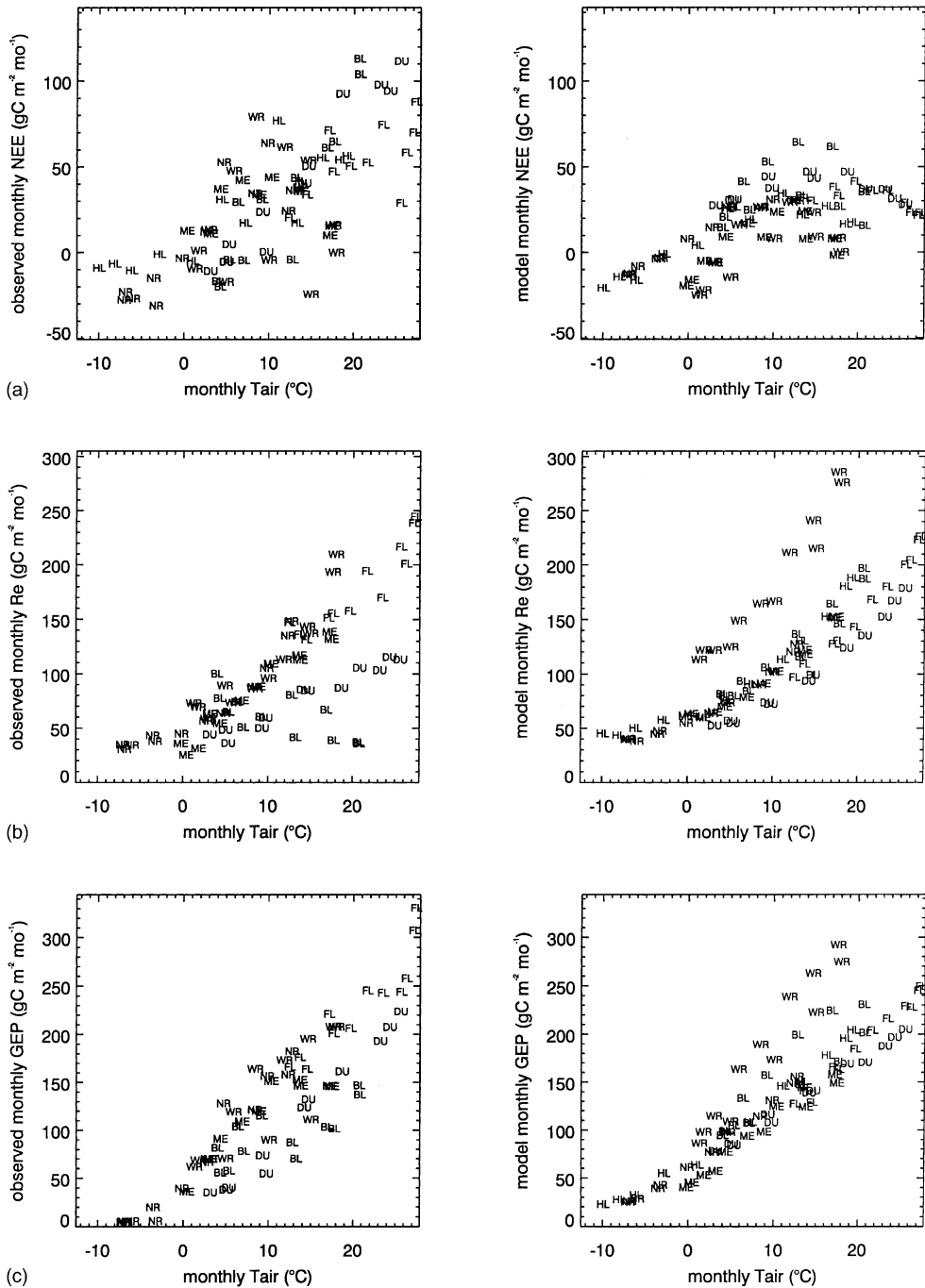


Fig. 12. Scatter-plots of observed and model monthly NEE (a),  $R_e$  (b) and GEP (c) vs. monthly average air temperature. Air temperatures are from the Daymet database. There is one symbol per site per month in each plot, except in the case of sites with no observations for a given month. Model values are the ensemble means from the final simulation year. Observed values are the average of all observations for a given month.

Table 7  
Observed ET<sup>a</sup>

Site	ET1	ET2	ET3
BL		664	664
DU	528	482	505
FL		988	988
HL	357	339	348
ME	521	444	482
NR	640	537	589
WR	542	443	493

<sup>a</sup> Shown are the average of annual ET estimates from Law et al. (2002) (ET1), the annual sum of averaged monthly values from Fig. 5b, where months with no data have been filled by linear interpolation (ET2) and the average of these two estimates (ET3). All units are in mm per year.

both the mean NEE and its standard error for each age class from this data. These estimates were compared to the modeled trajectory of NEE following a clear-cut (Fig. 15). Fig. 15 shows the annual total NEE measured for 2 years in each of three different aged stands using eddy covariance methods. Eddy covariance NEE measurements for the 10- and 11-year-old stands in Fig. 15 are the same data used for all previous analyses at the FL site in this study. The chronosequence data agree with the model results within the standard error of the observations, with no consistent pattern of bias. The chronosequence data also agree with the clear-cut and mid-rotation age eddy covariance measurements within the standard error of the chronosequence data, but the eddy covariance NEE is higher than the chronosequence estimate for the rotation-aged stand. These results demonstrate that the annual NEE for young and mid-aged stands from modeling and from flux measurements are both within the bounds

of measurement error for a nearby biometric analysis, even though the difference between them is relatively large. For the rotation-aged stands the chronosequence data are in better agreement with the modeled NEE than with the flux measurements.

At other sites it is clear that there is a fundamental discrepancy between the flux measurements and modeled annual values for NEE. For example, the observed value for current sink strength at ME ( $282 \text{ g C m}^{-2}$  per year  $\pm 180$ ) is more than two times higher than the peak sink strength predicted by the model, and that sink strength is only realized for about a decade within 30 years of a stand-replacing disturbance, which has not happened at the site for 250 years. Even with a large estimation error for the flux measurements of NEE and a range in current modeled NEE from interannual variation, there is still a minimum difference of  $50 \text{ g C m}^{-2}$  per year between model and flux measurements. A detailed analysis of model results at this site showed a close agreement with biometric measurements for multiple carbon budget component fluxes, as well as for one estimate of the net annual flux derived from those components (Law et al., 2001c). A Monte Carlo estimate using biometric data from the same study produced an NEE of  $170 \text{ g C m}^{-2}$  per year (S.D. 70), within the error of the flux measurements and higher than the model estimate. The Monte Carlo estimate is sensitive to variation in annual fine root production derived from different methods. Some measurement methods produce annual fine root production values that result in good agreement with the modeled NEE, and other methods result in NEE values closer to the flux measurements. The model is also very sensitive to the parameter defining the carbon

Table 8

Regression statistics and mean absolute errors (MAEs) for comparison of ET observations with two different summaries of model estimated ET<sup>a</sup>

Observed	Modeled	Slope	Intercept	R <sup>2</sup>	MAE (mm per year)	MAE (%)
ET1	ETm	0.57	291.5	0.06	157.2	29.6
ET1	ET*m	0.53	160.6	0.47	80.2	14.5
ET2	ETm	0.27	467.2	0.09	152.1	29.6
ET2	ET*m	0.43	246.1	0.74	99.4	14.8
ET3	ETm	0.31	438.5	0.10	153.2	27.4
ET3	ET*m	0.46	218.8	0.76	109.6	16.1

<sup>a</sup> Regressions were performed for each of ET1, ET2 and ET3 (Table 6), against the model total ET and the model total ET minus evaporation of canopy intercepted water (ET\*). Values for MAE are given both in mm per year and as percent of observed.

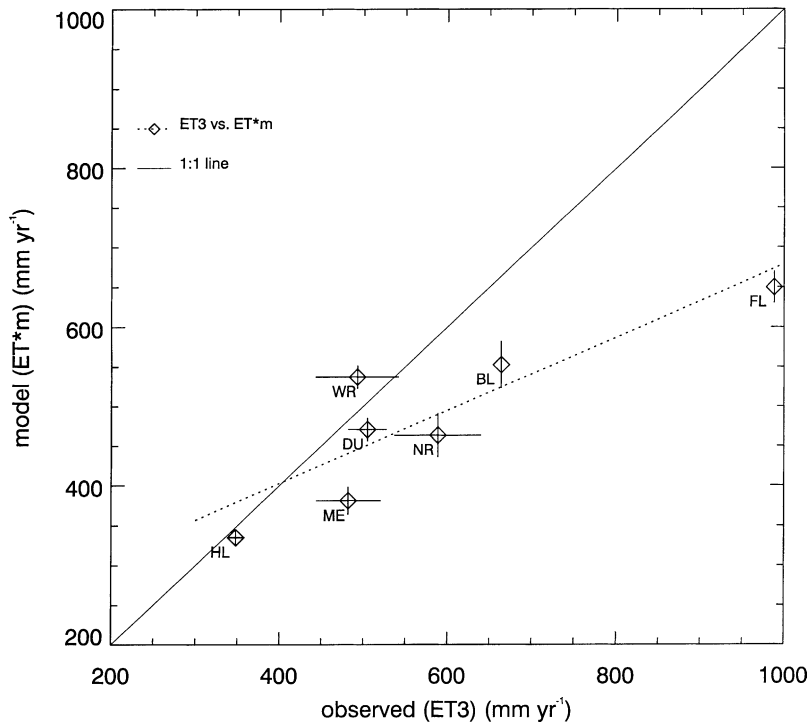


Fig. 13. Model (ET\*m) vs. observed (ET3) annual ET in the final simulation year. Error bars show interannual standard deviation for ensemble model results, and the results of two different calculation methods for the observations (ET1 and ET2).

allocation ratio between new fine roots and new leaves (Law et al., 2001c). More intensive study of belowground allocation patterns will be required to resolve the differences in NEE between the various measurement and modeling methods at this site. We do not yet know to what extent the same sensitivity exists for the other sites.

Recent biometric analyses at the WR site using Monte Carlo methods give an NEE of  $128 \text{ g C m}^{-2}$  per year  $\pm 100$ , but soil carbon stocks were ignored in the analysis (Harmon et al., in review). The modeled NEE is lower than the Monte Carlo estimate and the measured NEE (averaging  $192 \text{ g C m}^{-2}$  per year for 17 months of data) is higher, but both are within the Monte Carlo estimation error. Sensitivity tests show that model annual NEE is robust in the face of parameter uncertainty (results not shown). Since the model and flux estimates of NEE differ by more than  $150 \text{ g C m}^{-2}$  per year, it is possible that additional biometric analysis starting with a detailed baseline and focusing on changes in total

carbon stocks over time could resolve this discrepancy.

The fundamental argument against large annual sinks at the oldest sites, from a modeling perspective, is that unless the observed fluxes are unusual anomalies, and the recent mean of annual sink strength at these sites is much smaller, then the flux observations suggest that ecosystems at ME and WR should be accumulating carbon, either in the soil or in the vegetation, at a rate that is not compatible with the modeled dynamics of biomass accumulation and turnover to litter. For example, the current total ecosystem carbon content at WR is estimated at  $61.9 \text{ kg C m}^{-2}$  (Harmon et al., in review), and the stand age is around 450 years. Assuming that the entire ecosystem C pool is consumed in a stand-replacing fire, the average annual sink strength required to reach the current biomass in 450 years is  $137 \text{ g C m}^{-2}$  per year. This estimate is higher than the modeled NEE, within the range of the Monte Carlo estimate, and lower than the eddy flux measurements. Assuming a typical sigmoidal growth

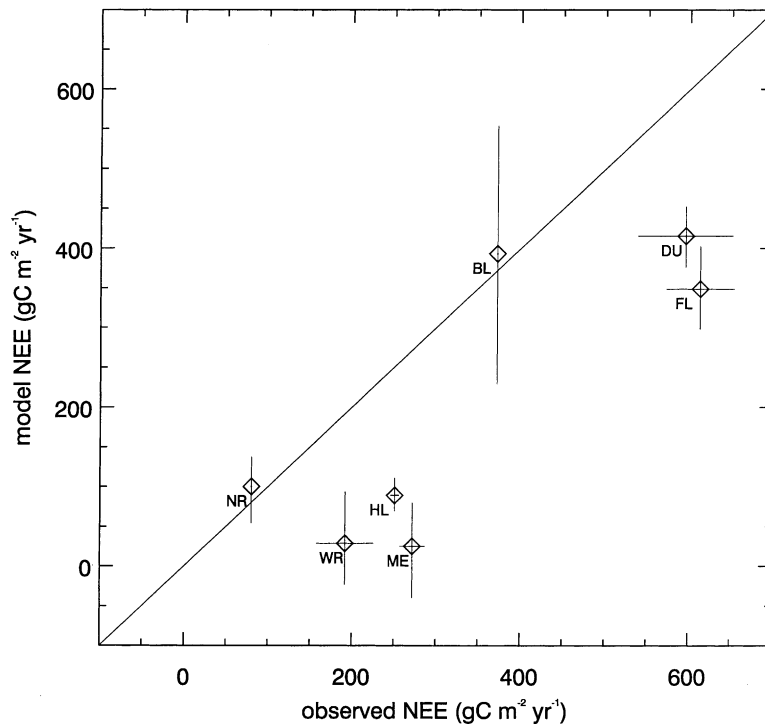


Fig. 14. Model vs. observed annual NEE in the final simulation year. Error bars show the interannual standard deviation for model ensemble results, and the range in observations when observations are available from multiple years.

curve for forest biomass accumulation, current accumulation rates should be substantially lower than this average. Making reasonable assumptions about the starting conditions for SOM, litter, and coarse woody debris (CWD) remaining after the stand-replacing disturbance reduces this estimate even further. It is possible that the fluxes observed at WR are not representative of the recent decadal mean, since the 2 years of observation are 1997–1998 during a strong El Niño event, and 1998–1999 during a strong La Niña event. Both winters were relatively mild, possibly contributing to unusually large sinks given the ability of the ecosystem to photosynthesize during periods of cool temperatures and predominantly diffuse radiation (Paw U et al., submitted).

The model estimates of winter respiration are higher than observed by soil chamber measurement at ME, and the model overestimates  $R_e$  at BL, DU, and WR, so it could be argued that the differences in observed and modeled annual NEE are because modeled  $R_e$  is seasonally or generally too high. The long-term patterns

of predicted NEE following disturbance are, however, surprisingly insensitive to this kind of variation, since high respiration leads to reduced carbon available for new growth, leading to reduced vegetation biomass and smaller litter inputs, eventually decreasing respiration. The peak sink strengths may change under these conditions, but the pattern of low net fluxes for old stands is maintained. If the base rates of respiration are changing transiently during the course of stand development, the pattern of NEE can shift significantly, but these changes are also reflected in the stand biomass, so they should be detectable with biometric analysis. It is likely that changes to the modeled respiration temperature responses would result in better agreement with the seasonal patterns of NEE from flux measurements, but further tests are required to know if these changes would also result in better agreement between the modeled and observed annual NEE.

At present, it is difficult to attribute the discrepancies between measured and modeled NEE to particular

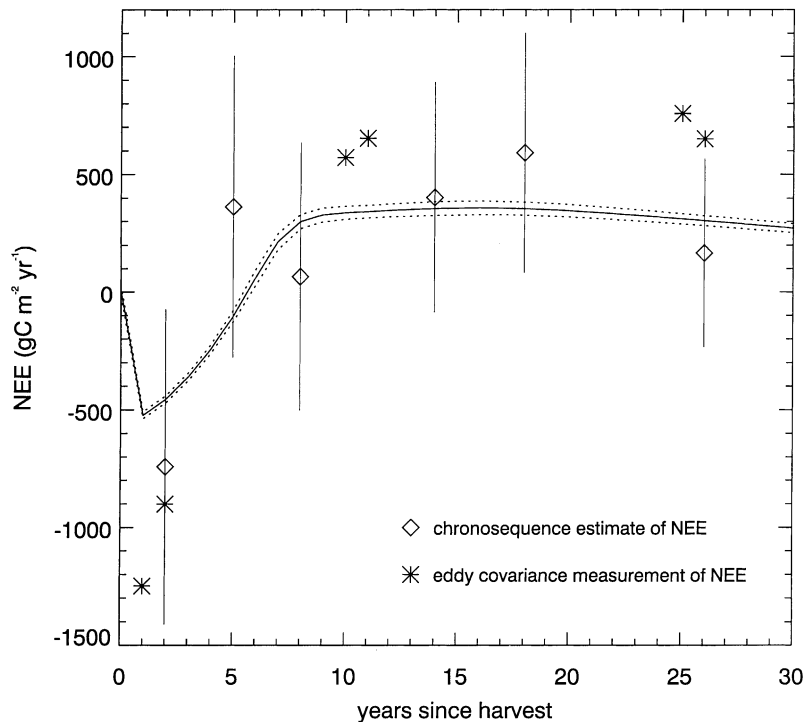


Fig. 15. Model ensemble mean (solid line) and interannual standard deviation (dotted line) for simulated NEE following harvest in a slash pine plantation at the FL site. Estimates of NEE from chronosequence data are shown, with standard errors estimated from individual plot data in [Gholz and Fisher \(1982\)](#) (see text). Eddy flux measurements of NEE are also shown, for measurements made at three different stand ages: immediately following clear-cut; in a mid-rotation-aged stand and in a rotation-aged stand.

deficiencies in either the model or the measurements. We would like to be able to explain both the differences in seasonal patterns of NEE ([Fig. 7](#)) and the differences in annual totals ([Fig. 14](#)). It seems likely that an explanation will include a combination of site-specific model parameterization problems (e.g., incorrect maximum stomatal conductance at FL, or incorrect treatment of respiration at low temperatures at ME), and site-specific measurement biases (e.g., undermeasurement of warm-season respiration at BL). The comparison of modeled and chamber-based estimates of  $R_e$  at ME is one useful approach to begin addressing these problems. Chamber-based estimates of respiration have been made at other sites, and additional comparisons between these data and modeled respiration should improve our understanding of differences between data and model by disaggregating the NEE signals. Detailed biometric analysis ([Law et al., 2001c](#)) also provides important additional

constraints on these interpretations, and should be pursued where data permit.

### 3.3. Model sensitivity tests

#### 3.3.1. Effects of woody biomass, litter, and SOM on disturbance recovery

Different disturbance types are defined in the model to have different effects on the pre-disturbance biomass, especially regarding the fate of woody material ([Appendix B](#)). For example, fire removes some woody biomass through combustion with the remainder entering the CWD pool, while harvest results in most of the woody biomass being removed. Slashburning following harvest eliminates even more woody material (coarse roots) and other fine litter generated from the harvest. Since the addition of large amounts of woody litter (with a high ratio of C:N) increases the modeled N immobilization potential, vegetation

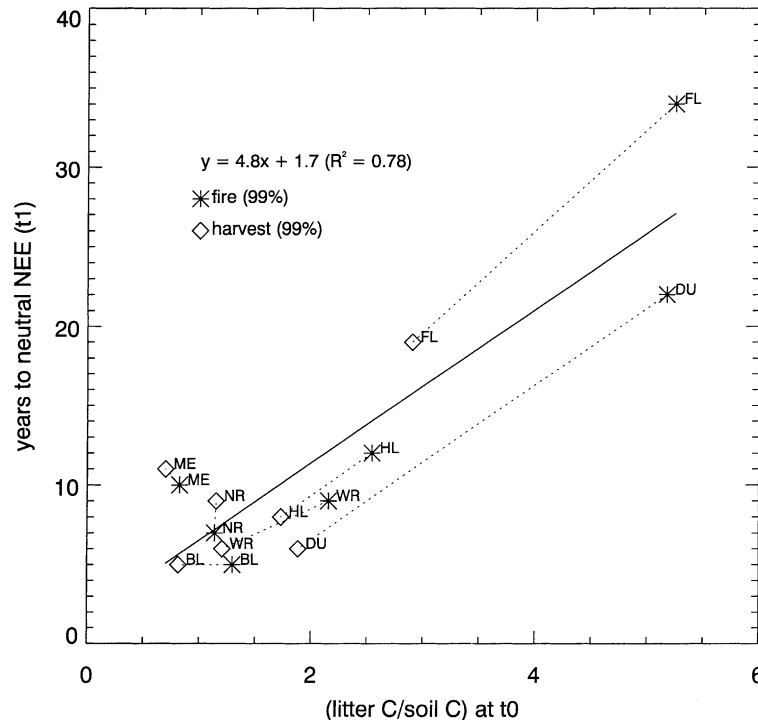


Fig. 16. Results of simple disturbance sensitivity tests, showing the time from disturbance until the site ensemble reached neutral NEE ( $t_1$ ) vs. the ratio of total carbon in litter (including CWD) to that in SOM measured at  $t_0$ , the time of disturbance. Regression line is shown (solid), and a dashed line connects the fire and harvest disturbances for each site to aid comparison of individual site responses to overall response.

recovery is slowed while regenerating plants compete with this demand for (usually limiting) mineral N resources.

A series of sensitivity tests was performed across the sites by applying simple harvest and fire disturbances from the spinup steady-state, and comparing the length of the source period and the total carbon lost during this period to the levels of woody debris remaining on site after the disturbance. In general, the duration of the net carbon source following a fire disturbance is greater than for a harvest disturbance affecting the same proportion of the biomass at the same site. This is in agreement with Monte Carlo simulations at WR using chronosequence measurements of aboveground live and dead pools and CWD decomposition rates only in the estimate (Janisch and Harmon, 2002). Considering only the 99% disturbance levels for fire and harvest, there is a strong relationship between the ratio of litter C/soil C immediately following disturbance and the length of the source period (Fig. 16).

Since soil C is closely related to the potential rate of soil N mineralization, and litter C is related to the N immobilization potential, this relationship supports the conclusion that N availability is limiting vegetation recovery rate when litter C is increased following disturbance.

Note that the source period following a 99% harvest disturbance for the sensitivity test in Fig. 16 is 18 years for FL, while the results in Fig. 3 show recovery in 4 years. The difference is due to slashburning, which removes some of the remaining CWD and replanting. Without these intensive treatments, the site is predicted to lose almost  $7000 \text{ g C m}^{-2}$  during the source period following a 99% harvest (Fig. 17), compared to a loss of about  $1500 \text{ g C m}^{-2}$  with the site treatments (s1 in Table 3). The model predicts that these treatments are required at the FL site to maintain soil fertility and site productivity for the characteristic 20–25-year harvest rotations on these plantations. Site treatments have less influence on disturbance recovery timing at DU and

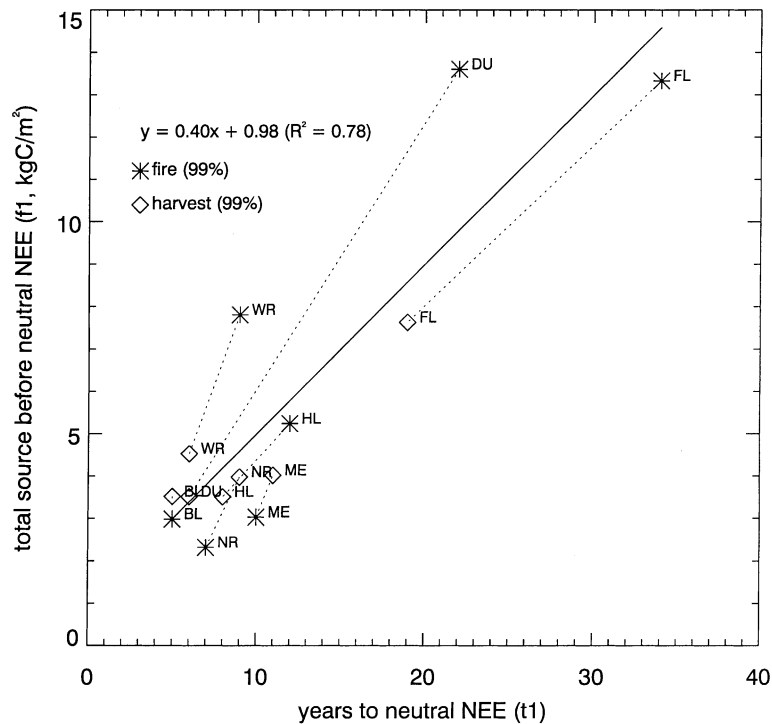


Fig. 17. Results of simple disturbance sensitivity tests, showing the total carbon source to the atmosphere during the period after disturbance until the site ensemble NEE reached neutrality, as a function of the time taken to reach neutral NEE. This source does not include carbon lost during the fire, or carbon removed from the site during harvest. Regression line is shown (solid), and a dashed line connects the fire and harvest disturbances for each site to aid comparison of individual site responses to overall response.

BL, although there is approximately a 30% reduction in total carbon loss during the source period due to replanting.

### 3.3.2. Effects of increasing atmospheric $CO_2$ and $N_{dep}$ on disturbance recovery

The difference between NEE predicted with observed trends in  $CO_2$  and  $N_{dep}$  superimposed on site disturbance history, and NEE predicted with  $CO_2$  and  $N_{dep}$  constant at pre-industrial levels is shown as a time series for each site in Fig. 18. The values in parentheses in Table 3 summarize these differences by site. In general, the influence of higher  $CO_2$  concentration and higher atmospheric inputs of mineral N is to reduce the length of the source period following disturbance, reduce the total carbon loss during this period, reduce the time to reach peak sink strength, increase this sink strength, and also increase the peak source strength. The net effect is an increase

in total system carbon storage over the entire historical period for all sites. The degree of these effects depends on the  $CO_2$  concentration and the level of N deposition at the time of disturbance. Recent disturbances showed larger interactions with  $CO_2$  and  $N_{dep}$ .

The modeled interaction between disturbance response and atmospheric chemistry is related to the availability of mineral N to support new plant growth. At some point in the simulation after disturbance, while plant biomass is still low (keeping plant N demand low) and decomposition of litter produced during the disturbance has progressed to a net mineralization phase, the N limitation to new growth drops and plant growth accelerates. If this occurs when the  $CO_2$  concentration is high the plants can take advantage of the increased carboxylation potential while still satisfying basic stoichiometric requirements for N, and growth is stimulated.

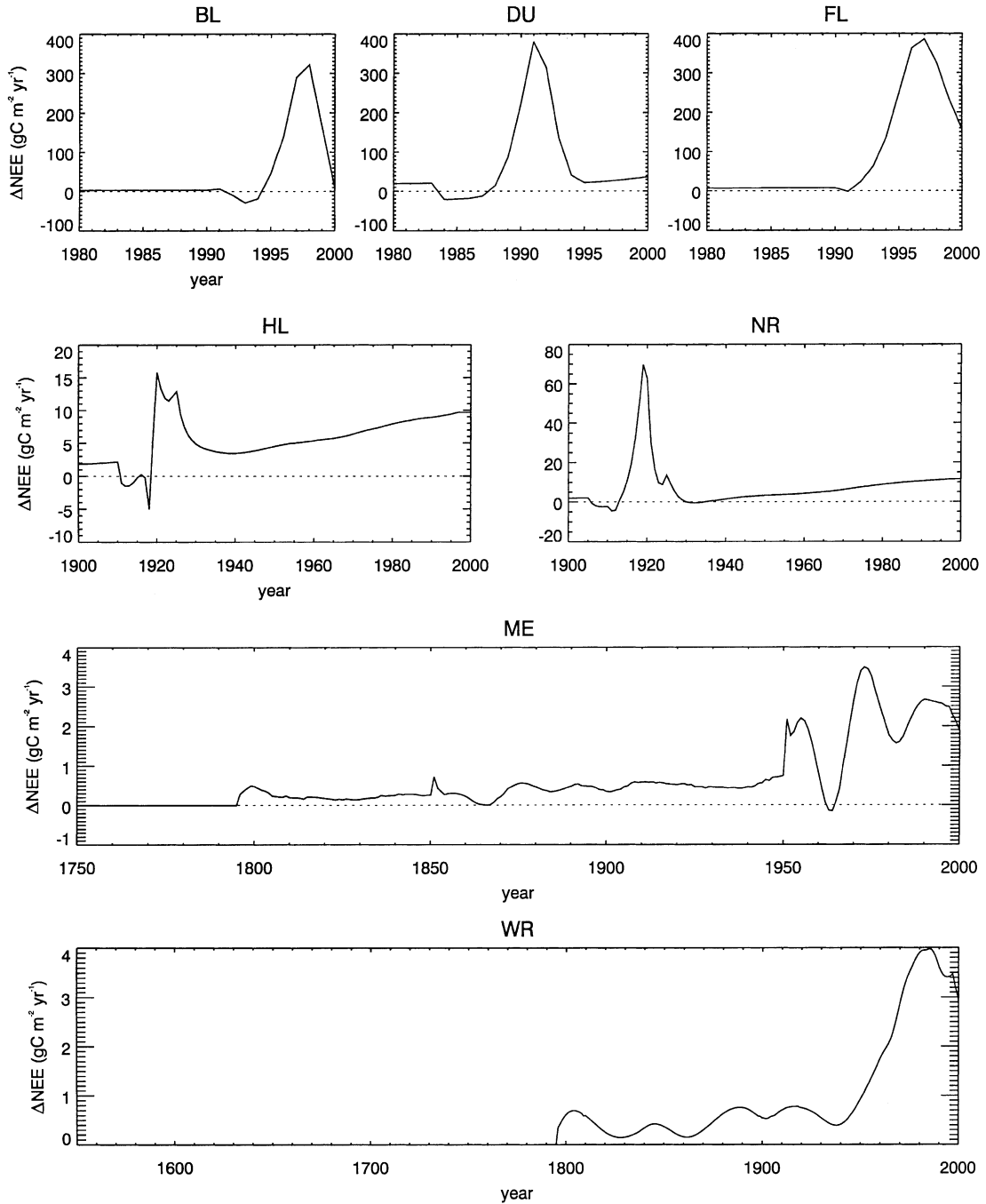


Fig. 18. Time series of the effect of historical increases in atmospheric concentration of CO<sub>2</sub> and changes in total mineral N deposition on NEE for each study site. Time axis for each site is as in Fig. 3, but here the y-axis has been scaled independently for each site to better show detailed site responses. Plotted are the difference in ensemble mean NEE for observed changes in CO<sub>2</sub> and N<sub>dep</sub> minus the ensemble mean NEE for simulations holding CO<sub>2</sub> and N<sub>dep</sub> constant at their pre-industrial levels (circa 1796). Large responses following disturbance show the interaction effect of disturbance recovery dynamics and fertilization by CO<sub>2</sub> and mineral N deposition.

An interesting result from these simulations is that when  $N_{\text{dep}}$  is constant and recent disturbance is minimal (e.g., at ME and WR), NEE is responding not to the absolute concentration of atmospheric  $\text{CO}_2$  but to the rate of change in atmospheric  $\text{CO}_2$  concentration over time. These results are especially clear for WR (Fig. 18), where the variation in NEE corresponds almost entirely to the rate of change of  $\text{CO}_2$  in the IS92a scenario. These NEE effects are also quite small, amounting to about  $200 \text{ g C m}^{-2}$  total increase in system C storage over 200 years. A likely explanation is that gains in NPP are quickly translated to increases in litter mass and heterotrophic respiration, so that the net effect is small on the time scale similar to the leaf longevity, with some longer memory due to new woody allocation. To sustain a net sink, the  $\text{CO}_2$  concentration must be increasing with time. For the net sink to increase over time, the *rate of increase* in  $\text{CO}_2$  concentration must be increasing over time. Increases in  $N_{\text{dep}}$  for these chronically N-limited systems dominate the  $\text{CO}_2$  response (except at FL), as can be seen in the recent history at DU, a site with high current  $N_{\text{dep}}$ .

Although the effect of current levels of  $\text{CO}_2$  and  $N_{\text{dep}}$  can be very large during the shift from source to sink after disturbance (up to  $400 \text{ g C m}^{-2}$  per year), they do not last longer than about a decade at those levels. All of the sites are predicted to be past the peak effect for the most recent disturbances. The modeled interactions between  $\text{CO}_2$  fertilization, N availability, and disturbance are highly non-linear. It is difficult to predict the level of  $N_{\text{dep}}$  at which a colimitation with  $\text{CO}_2$  might be reached for a given climate, vegetation physiology, and temporal pattern of disturbance. At that point we would expect to see rapid changes in NEE with small additional changes in  $N_{\text{dep}}$ ,  $\text{CO}_2$ , or disturbance frequency or intensity. Especially for regions of high current rates of  $N_{\text{dep}}$ , these non-linear interactions warrant further study.

#### 4. Conclusions

The model simulations suggest that there is a consistent pattern of early carbon source followed by strong and gradually diminishing sink during recovery from a major disturbance. These dynamics are modified by the site climate and by characteristics of

the vegetation such as leaf longevity. Recovery time is longer when the amount of litter material is large compared to the amount of SOM immediately after disturbance. The effects of  $\text{CO}_2$  and  $N_{\text{dep}}$  on NEE are strongest during the rapid regrowth phase following disturbance because of changes during that period in mineral N demand and availability. The fertilization effects depend on the degree of colimitation between mineral N availability and carboxylation potential at each site. At sites with old stands and small changes in the rate of  $N_{\text{dep}}$ , model NEE responds to the rate of change in atmospheric  $\text{CO}_2$ . This means that, in the absence of recent disturbance events, an increasing sink strength due to  $\text{CO}_2$  fertilization over time depends mostly on an increasing rate of accumulation of  $\text{CO}_2$  in the atmosphere.

Model results suggest that management practices following harvest at three sites are playing an important role in the disturbance recovery response of NEE, by reducing the amount of CWD with slashburning and advancing the competitiveness of plants for available mineral N resources with replanting (Schulze et al., 2000). It is not clear what the long-term or multiple rotation implications of these management practices are for the site carbon budgets.

Model estimates of LAI compared well with observations across the wide climatic range for the study sites. ET comparisons at WR suggest an important difference between the modeled and observed evaporation of water from the wet canopy at this high-LAI site. The available data is not sufficient to distinguish between potential biases in the model and in the measurements for wet canopy evaporation. Summer ET comparisons from the three young stands suggest that the model stomatal conductance was too low at these sites, while seasonal patterns of ET at several sites agreed well with observations (Chen et al., 2002).

Model estimates of NEE and its components compared moderately well at NR, but there is a strong model underestimation of sink strength at most sites during the warm season. It is possible that the modeled temperature dependence for autotrophic and/or heterotrophic respiration is inaccurate, causing the observed difference in seasonal patterns of NEE between model results and flux measurements. Additional comparisons using available chamber measurements from other sites will be an important next step in resolving these differences.

The measurement uncertainty for belowground allocation of carbon is large, and the model is known to be sensitive to the parameterization of this process: less allocation belowground as stands age results in less autotrophic and heterotrophic respiration and greater simulated annual NEE (Law et al., 2001c). Here we assumed that carbon allocation patterns remained the same as stands age, but field data show that this is not the case. The measurement uncertainties will have to be reduced before an accurate parameterization of this process can be included in the model. Until then, it is valuable to continue to assess the influence of variation in this parameter on modeled NEE.

These simulations and comparisons have demonstrated the possibility that the details of disturbance history provide a dominant constraint on the net exchange of carbon at decadal and longer time scales. This suggests that disturbance history will be an important component of studies examining feedback through the carbon cycle between the terrestrial biosphere and other components of the climate system.

## Acknowledgements

P.E. Thornton was supported by NASA (grant no. W-19,953), NSF (grant no. DEB-9977066), USGS (grant no. 99CRAG0063) and the National Center for Atmospheric Research (NCAR), Boulder, CO. NCAR is sponsored by the National Science Foundation. B.E. Law was supported by NASA (grant no. NAG5-7531), and DOE (grant no. FG0300ER63014). We acknowledge the efforts of many people in the field data collection at the sites, analysis, and synthesis, including P. Anthony, D. Moore and S. Van Tuyl.

## Appendix A

*Biome-BGC process descriptions.* Many of the principle physical and biological processes represented in Biome-BGC are summarized below. The computer code itself contains extensive and explicit comments for all processes, as well as detailed descriptions of all model state and flux variables, including units and unit conversions. The code is available by request from P.E. Thornton. This study used version 4.1.1 of the Biome-BGC code.

*Canopy radiation.* The plant canopy leaf area is divided into sunlit and shaded fractions on the basis of a radiation extinction coefficient that varies with leaf geometry. All plant physiological processes are calculated separately for the sunlit and shaded canopy fractions. Differences in leaf physiology between the sunlit and shaded fractions are parameterized as differences in SLA, with the mass-based nitrogen concentration and controls on stomatal conductance constant between sunlit and shaded fractions.

*Photosynthesis.* Assimilation ( $A$ ) on a unit projected leaf area basis for C3 plants is estimated independently for the sunlit and shaded canopy fractions, using a biochemical model (Farquhar et al., 1980, with kinetic parameters from Woodrow and Berry (1988), de Pury and Farquhar (1997)) and substitution from the  $\text{CO}_2$  diffusion equation to eliminate the explicit dependency on intracellular  $\text{CO}_2$  concentration. The maximum rate of carboxylation ( $V_{C,\max}$ ) is calculated as a function of the specific activity of the Rubisco enzyme (act, itself a function of leaf temperature), the weight fraction of nitrogen in the Rubisco molecule (fnr), the fraction of total leaf nitrogen in the Rubisco enzyme (flnr), the specific leaf area (sla), and the leaf C:N ratio ( $C:N_{\text{leaf}}$ ) as follows (dimensional analysis to the right):

$$V_{C,\max} = \frac{\text{act} \times \text{flnr}}{\text{fnr} \times \text{sla} \times C : N_{\text{leaf}}},$$

$$\left( \frac{\mu\text{mol CO}_2}{\text{m}^2 \text{ s}} \right) = \frac{(\mu\text{mol CO}_2/\text{g Rubisco s}) \times (\text{g } N_{\text{Rubisco}}/\text{g } N_{\text{leaf}})}{(\text{g } N_{\text{Rubisco}}/\text{g Rubisco}) \times (\text{m}^2/\text{g } C_{\text{leaf}})(\text{g } C_{\text{leaf}}/\text{g } N_{\text{leaf}})}$$

The model is very sensitive to the value for flnr, and when data is available we optimize this parameter by fitting to  $A-C_i$  curves. This approach requires knowing the leaf temperature as well as sla and  $C:N_{\text{leaf}}$  for the measured leaves. One advantage of this formulation is that it makes explicit the dependence of  $V_{C,\max}$  on sla and  $C:N_{\text{leaf}}$ . Values for fnr and act, as well as the temperature dependence of act, are assumed constant across all species.

*Stomatal conductance.* A form of the Leuning model is used, which makes actual conductance a function of a minimum value and a series of multiplicative reductions based on incident radiation, vapor pressure deficit, leaf water potential, and night minimum temperature (Running and Coughlan, 1988).

There is no direct effect of changing atmospheric CO<sub>2</sub> concentration on stomatal conductance, which is in agreement with recent studies for woody vegetation (Norby et al., 1999). One practical benefit of this formulation is that it is not necessary to iterate between the equations for CO<sub>2</sub>, water, and energy transfer at the leaf surface, as is the case, e.g., with the Ball-Berry model in which stomatal conductance is an explicit function of carbon assimilation.

*Evaporation and transpiration.* Both processes are estimated using the Penman–Monteith equation. Available energy is partitioned between the canopy and the soil surface. Soil evaporation depends on the number of days since wetting. Energy available in the canopy is divided between the evaporation of water intercepted on the canopy and transpiration. Both these processes depend on the leaf-scale aerodynamic conductance, with transpiration depending in addition on stomatal conductance.

*Autotrophic respiration.* Two types of autotrophic respiration are distinguished—maintenance respiration, which is calculated as a function of tissue mass, tissue nitrogen concentration, and tissue temperature, and growth respiration which is a simple proportion of total new carbon allocated to growth. Maintenance respiration costs are incurred regardless of current assimilation rate.

*Phenology.* For all vegetation types, some growth can be stored for display during the following growing season. For this stored growth, the model developed by White et al. (1997) is used to estimate the middle of the leaf expansion and litterfall periods for deciduous broadleaf trees and for grasses. For all vegetation types the user has the option to specify the proportion of the total growing season during which stored growth is displayed. The growth that is not stored for display in the following growing season is displayed immediately, and so the overall seasonal growth signal consists of one component due to stored growth and a second component due to current growth. The current growth component has a strong dependency on the stored growth, since the stored growth augments the canopy leaf area and changes the growth potential independent of the current growing season conditions. This is essential to the development of new canopy in the spring for a deciduous system, and is also important for evergreen vegetation.

*Allocation of carbon and nitrogen.* The C:N stoichiometry of new plant allocation is constant, defined by ratios between allocation to new leaf and to each of the other plant tissues (fine root, live and dead stem wood, live and dead coarse root wood). The C:N stoichiometry of total plant biomass changes over time as leaves and fine roots turn over to litter pools, while wood accumulates. All plant pools for C and N are completely prognostic, so leaf area responds to changes in climate, physiological parameterizations, disturbance regimes, and dynamics in the SOM pools over time. The availability of C from assimilation and the availability of N from plant mineral N uptake must be balanced to meet this constant C:N for new growth, which is achieved by down-regulating assimilation under conditions of chronic N limitation.

*Plant mineral nitrogen uptake.* Plants compete with the N immobilizing processes in the litter and soil decomposition dynamics for one pool of soil mineral N. This competition is based on relative demand, which is set by the plant's potential assimilation rate and the potential N immobilization rate due to decomposition, both estimated assuming current values for all the state variables. Actual assimilation and actual decomposition then proceed at either their potential rates if mineral N is not limiting, or at reduced rates if N is limiting.

*Litter and SOM pools.* All plant litter is divided into three pools on the basis of the weight fractions of lignin, cellulose plus hemicellulose, and remaining mass in the litter. These litter pools undergo chemical degradation at different rates, producing a connected series of SOM pools. The model structure defines a converging cascade of progressively more recalcitrant SOM (Thornton, 1998). Before entering the active litter pools, woody litter passes through a CWD pool that is subject only to physical degradation. C:N ratios for the litter pools depend on the inputs from plants, but C:N ratios for the SOM pools are fixed.

*Heterotrophic respiration.* Litter and SOM decomposition produces a heterotrophic respiration flux, which depends on the size of the litter and SOM pools and their decomposition rate constants. These rate constants depend on soil temperature and soil moisture. Decomposition also depends on the availability of soil mineral N for those steps which are immobilizing N (see description of plant N uptake above).

Table B.1  
Parameters that vary between sites

No.	Units	Description
1	yr <sup>-1</sup>	Annual turnover proportion for leaves and fine roots
2	dim	New fine root C allocation:new leaf C allocation
3	dim	New stem C allocation:new leaf C allocation
4	dim	New coarse root C allocation:new stem C allocation
5	kg C kg N <sup>-1</sup>	C:N of current year's foliage at maturity
6	kg C kg N <sup>-1</sup>	C:N of fresh leaf litter, after retranslocation
7	kg C kg N <sup>-1</sup>	C:N of fine roots
8	kg C kg N <sup>-1</sup>	C:N of dead wood
9	prop	Leaf litter lignin proportion
10	prop	Fine root lignin proportion
11	m <sup>2</sup> kg C <sup>-1</sup>	Canopy average SLA—projected leaf area basis
12	m s <sup>-1</sup>	Maximum stomatal conductance—projected leaf area basis

### Appendix B. Site-specific ecophysiological parameters for Biome-BGC

The parameters used to describe vegetation ecophysiology in Biome-BGC are listed in Table B.1, with their units and description. For further details, see White et al. (2000). Units indicated as (dim) are dimensionless ratios; units indicated as (prop) are proportions. The value of each parameter at each site is given in Table B.2. There are a number of parameters that were not varied between sites, and values, units, and descriptions for these are given in Table B.3.

### Appendix C. Definition of disturbance effects on model state variables

Each disturbance type was defined by its action on the model state variables for carbon and nitrogen.

Within each type a single parameter was used to specify the disturbance level.

*Fire.* All plant and fine litter state variables are affected as a proportion of their initial values immediately before the disturbance. The affected proportions of the leaf, fine root, live wood, and fine litter C and N pools are assumed to be consumed in the fire and lost to the atmosphere. The affected proportions of the dead wood C and N pools are sent to the CWD pools, which are then subjected to combustion losses to the atmosphere at half the specified proportion. The reduced effect on CWD pools is intended to address the fact that most burns do not consume all of the large woody material on a site. Slashburning as a management practice is treated simply as a fire of a specified proportion following a harvest disturbance.

*Harvest.* All plant state variables are affected as a proportion of their initial values immediately before the disturbance. The affected proportions of the leaf

Table B.2  
Site-specific values for parameters from Table 9

Parameter no.	BL	DU	FL	HL	ME	NR	WR
1	0.33	0.5	0.5	0.2	0.25	0.2	0.167
2	1.0	0.15	0.7	1.0	2.5	1.0	1.0
3	1.0	2.35	1.7	2.0	1.0	2.0	2.0
4	0.1	0.1	0.28	0.2	0.14	0.2	0.1
5	50	43	45	40	50	40	45
6	92	107	80	100	92	100	92
7	79	55	55	55	79	55	79
8	300	300	460	300	300	300	600
9	0.41	0.41	0.26	0.3	0.41	0.3	0.2
10	0.42	0.42	0.25	0.2	0.42	0.2	0.2
11	7.7	10.6	5.7	10.0	7.7	10.0	10.0
12	0.002	0.0015	0.003	0.0015	0.002	0.0015	0.0015

Table B.3

Parameters given the same value at all sites

Value	Units	Description
0.7	yr <sup>-1</sup>	Annual turnover proportion for live wood
0.005	yr <sup>-1</sup>	Annual non-fire mortality proportion
0.01	yr <sup>-1</sup>	Annual fire mortality proportion
0.5	prop	Proportion of daily production allocated to currently displayed growth, remainder stored for display the following year
50	kg C kg N <sup>-1</sup>	C:N of live wood (phloem)
0.24	prop	Dead wood lignin proportion
0.01	m <sup>-2</sup> per day	Canopy water interception coefficient—proportion of total rainfall captured on the canopy and available for evaporation, per unit projected leaf area per day
0.5	dim	Canopy light extinction coefficient
2.36	dim	Ratio of all-sided to projected leaf area
2.0	dim	Ratio of SLA in shaded to sunlit canopy
0.06	prop	Proportion of leaf N in the Rubisco enzyme
3.0E-5	m s <sup>-1</sup>	Leaf cuticular conductance—projected area basis
0.1	m s <sup>-1</sup>	Leaf boundary layer conductance—projected area basis
-0.6	MPa	Pre-dawn leaf water potential at start of stomatal conductance reduction
-2.3	MPa	Pre-dawn leaf water potential at complete stomatal conductance reduction
610	Pa	Vapor pressure deficit at start of stomatal conductance reduction
3100	Pa	Vapor pressure deficit at complete stomatal conductance reduction

and fine root C and N pools are sent to the fine litter. The affected proportions of aboveground live and dead wood C and N pools are assumed removed from the site, and no longer enter into the site mass balance. The affected proportions of belowground live and dead wood C and N pools are sent to the CWD pools.

**Replanting.** This management practice is treated as the addition of a specified mass ( $m$ ) to the storage pool for leaf C, with an addition to the storage pool for leaf N determined by  $m$  and the specified leaf C:N. The storage pools are transferred to displayed growth during the subsequent growing season.

## References

- Chen, J., Falk, M.M., Paw U, K.T., Suchanek, T., Ustin, S., Bond, B., Phillips, N., Brosofske, K., Euskirchen, E., 2002. Biophysical controls of carbon flows in three successional Douglas-fir stands based upon eddy-covariance method. *Tree Phys.* 22 (2/3), 171–180.
- Clark, K., Gholz, H.L., Moncrieff, J.B., Cropley, F., Loescher, H.W., 1999. Environmental controls over net exchanges of carbon dioxide from contrasting Florida ecosystems. *Ecol. Applic.* 9, 936–948.
- de Pury, D.G.G., Farquhar, G.D., 1997. Simple scaling of photosynthesis from leaves to canopies without the errors of big-leaf models. *Plant Cell Environ.* 20, 537–557.
- Denning, A.S., Fung, I.Y., Randall, D., 1995. Latitudinal gradient of atmospheric CO<sub>2</sub> due to seasonal exchange with land biota. *Nature* 376, 240–243.
- Enting, I.G., Wigley, T.M.L., Heimann, M., 1994. Future emissions and concentrations of carbon dioxide: key ocean/atmosphere/land analyses. Technical Paper 31. Division of Atmospheric Research, CSIRO, Melbourne, Australia.
- Falge, E., Baldocchi, D., Tenhunen, J., Aubinet, M., Bakwin, P., Berbigier, P., Bernhofer, C., Burba, G., Clement, R., Davis, K.J., Elbers, J.A., Goldstein, A.H., Grelle, A., Granier, A., Guðmundsson, J., Hollinger, D., Kowalski, A.S., Katul, G., Law, B.E., Malhi, Y., Meyers, T., Monson, R.K., Munger, J.W., Oechel, W., Paw U, K.T., Pilegaard, K., Rannik, U., Rebmann, C., Suyker, A., Valentini, R., Wilson, K., Wofsy, S., 2002. Seasonality of ecosystem respiration and gross primary production as derived from fluxnet measurements. *Agric. For. Meteorol.* 113, 53–74.
- Farquhar, G.D., von Caemmerer, S., Berry, J.A., 1980. A biochemical model of photosynthetic CO<sub>2</sub> assimilation in leaves of C<sub>3</sub> species. *Planta* 149, 78–90.
- Fassnacht, K.S., Gower, S.T., Norman, J.M., McMurtrie, R.E., 1994. A comparison of optical and direct methods for estimating foliage surface area index in forests. *Agric. For. Meteorol.* 71, 183–207.
- Gholz, H.L., Fisher, R.F., 1982. Organic matter production and distribution in slash pine (*Pinus elliottii*) plantations. *Ecology* 63 (6), 1827–1839.
- Gholz, H.L., Perry, C.S., Cropper, W.P., Hendry, L.C., 1985. Litterfall, decomposition, and nitrogen and phosphorus dynamics in a chronosequence of Slash Pine (*Pinus elliottii*) plantations. *For. Sci.* 31, 463–478.

- Gholz, H.L., Vogel, S.A., Cropper, W.P., McKelvey, K., Ewel, K.C., Teskey, R.O., Curran, P.J., 1991. Dynamics of canopy structure and light interception in *Pinus elliottii* stands, North Florida. *Ecol. Monogr.* 61, 33–51.
- Hansen, M.C., DeFries, R.S., Townsend, J.R.G., Sohlberg, R., 2000. Global land cover classification at 1 km spatial resolution using a classification tree approach. *Int. J. Remote Sens.* 21, 1331–1364.
- Harmon, M., Garman, S.L., Ferrell, W.K., 1996. Modeling historical patterns of tree utilization in the Pacific northwest: carbon sequestration implications. *Ecol. Appl.* 6, 641–652.
- Harmon, M., Bible, K., Ryan, M.J., Shaw, D., Chen, H., Klopfatek, J., in review. Production, respiration, and overall carbon balance in an old-growth *Pseudotsuga/Tsuga* forest ecosystem. *Ecosystems*.
- Hollinger, D.Y., Goltz, S.M., Davidson, E.A., Lee, J.T., Tu, K., Valentine, H.T., 1999. Seasonal patterns and environmental control of carbon dioxide and water vapour exchange in an ecotonal boreal forest. *Global Change Biol.* 5, 891–902.
- Janisch, J.E., Harmon, M.E., 2002. Successional changes in live and dead wood stores: Implications for net ecosystem productivity. *Tree Physiol.* 22, 77–89.
- Kimball, J.S., Thornton, P.E., White, M.A., Running, S.W., 1997. Simulating forest productivity and surface-atmosphere exchange in the BOREAS study region. *Tree Physiol.* 17, 589 and 599.
- Kucharik, C.J., Foley, J.A., Delire, C., Fisher, V.A., Coe, M.T., Lenters, J.D., Young-Molling, C., Ramankutty, N., Norman, J.M., Gower, S.T., 2000. Testing the performance of a dynamic global ecosystem model: water balance, carbon balance, and vegetation structure. *Global Biogeochem. Cycles* 14 (3), 795–825.
- Law, B.E., Baldocchi, D.D., Anthoni, P.M., 1999. Below-canopy and soil CO<sub>2</sub> fluxes in a ponderosa pine forest. *Agric. For. Meteorol.* 94, 171–188.
- Law, B.E., Van Tuyl, S., Cescatti, A., Baldocchi, D.D., 2001a. Estimation of leaf area index in open-canopy ponderosa pine forests at different successional stages and management treatments in Oregon. *Agric. For. Meteorol.* 108, 1–14.
- Law, B.E., Cescatti, A., Baldocchi, D.D., 2001b. Leaf area distribution and radiative transfer in open-canopy forests: implications to mass and energy exchange. *Tree Physiol.* 21, 777–787.
- Law, B.E., Thornton, P.E., Irvine, J., Van Tuyl, S., Anthoni, P.M., 2001c. Carbon storage and fluxes in ponderosa pine forests at different developmental stages. *Global Change Biol.* 7, 755–777.
- Law, B.E., Flage, E., Gu, L., Baldocchi, D.D., Bakwin, P., Berbigier, P., Davis, K., Dolman, A.J., Falk, M., Fuentes, J.D., Goldstein, A., Granier, A., Grelle, A., Hollinger, D., Janssens, I.A., Jarvis, P., Jensen, N.O., Katul, G., Mahli, Y., Matteucci, G., Meyers, T., Monson, R., Munger, W., Oechel, W., Olson, R., Pilegaard, K., Paw U, K.T., Thorgeirsson H., Valentini, R., Verma, S., Vesala, T., Wilson, K., Wofsy, S., 2002. Environmental controls over carbon dioxide and water vapor exchange of terrestrial vegetation. 113, 97–120.
- McGuire, A.D., Melillo, J.M., Joyce, L.A., Kicklighter, D.W., Grace, A.L., Moore III, B., Vorosmarty, C.J., 1992. Interactions between carbon and nitrogen dynamics in estimating net primary productivity for potential vegetation in North America. *Global Biogeochem. Cycles* 6 (2), 101–124.
- McGuire, A.D., Sitch, S., Clein, J.S., Dargaville, R., Esser, G., Foley, J., Heimann, M., Joos, F., Kaplan, J., Kicklighter, D.W., Meier, R.A., Melillo, J.M., Moore III, B., Prentice, I.C., Ramankutty, N., Reichenau, T., Scloss, A., Tian, H., Williams, L.J., Wittenberg, U., 2001. Carbon balance of the terrestrial biosphere in the twentieth century: analyses of CO<sub>2</sub>, climate, and land use effects with four process-based ecosystem models. *Global Biogeochem. Cycles* 15 (1), 183–206.
- NADP (National Atmospheric Deposition Program) (NRSP-3)/ National Trends Network, 2000. NADP Program Office, Illinois State Water Survey, 2204 Griffith Dr., Champaign, IL.
- Norby, R.J., Wullschlegel, S.D., Gunderson, C.A., Johnson, D.W., Ceulmans, R., 1999. Tree responses to rising CO<sub>2</sub> in field experiments: implications for the future forest. *Plant Cell Environ.* 22, 683–714.
- Paw U, K.T., Falk, M., Suchanek, T.H., Ustin, S.L., Chen, J., Park, Y.S., Winner, W.E., Thomas, S.C., Hsiao, T.C., Shaw, R.H., King, T.S., Pyles, R.D., Matista, A.A., submitted. Carbon dioxide exchange between an old growth forest and the atmosphere. *Ecosystems*.
- Running, S.W., Coughlan, J.C., 1988. A general model of forest ecosystem processes for regional applications. I. Hydrological balance, canopy gas exchange and primary production processes. *Ecol. Model.* 42, 125–154.
- Schimel, D.S., Alves, D., Enting, I., Heimann, M., Joos, F., Raymond, D., Wigley, T., 1996. CO<sub>2</sub> and the carbon cycle, in: Houghton, J.T., et al. (Eds.), *Climate Change 1995*. Cambridge University Press, New York, pp. 76–86.
- Schimel, D.S., Melillo, D.J., Tian, H., McGuire, A.D., Kicklighter, D., Kittel, T., Rosenbloom, N., Running, S., Thornton, P., Ojima, D., Parton, W., Kelly, R., Sykes, M., Neilson, R., Rizzo, B., 2000. Contribution of increasing CO<sub>2</sub> and climate to carbon storage by ecosystems in the United States. *Science* 287, 2004–2006.
- Schulze, E.-D., Wirth, C., Heiman, M., 2000. Managing forests after Kyoto. *Science* 289, 2058–2059.
- Stenberg, P., 1996. Correcting LAI-2000 estimates for the clumping of needles in shoots of conifers. *Agric. For. Meteorol.* 79, 1–8.
- Thornton, P.E., 1998. Regional ecosystem simulation: combining surface- and satellite-based observations to study linkages between terrestrial energy and mass budgets. Ph.D. dissertation. School of Forestry, University of Montana, Missoula MT, 280 pp.
- Thornton, P.E., Running, S.W., 1999. An improved algorithm for estimating incident daily solar radiation from measurements of temperature, humidity, and precipitation. *Agric. For. Meteorol.* 93, 211–228.
- Thornton, P.E., Running, S.W., White, M.A., 1997. Generating surfaces of daily meteorological variables over large regions of complex terrain. *J. Hydrol.* 190, 214–251.
- Thornton, P.E., Hasenauer, H., White, M.A., 2000. Simultaneous estimation of daily solar radiation and humidity from observed temperature and precipitation: an application of complex terrain in Austria. *Agric. For. Meteorol.* 104, 255–271.

- White, M.A., Thornton, P.E., Running, S.W., 1997. A continental phenology model for monitoring vegetation responses to interannual climatic variability. *Global Biogeochem. Cycles* 11 (2), 217–234.
- White, M.A., Thornton, P.E., Running, S.W., Nemani, R.R., 2000. Parameterization and sensitivity analysis of the Biome-BGC terrestrial ecosystem model: net primary production controls. *Earth Interactions* 4 (3), 1–85.
- Woodrow, I.E., Berry, J.A., 1988. Enzymatic regulation of photosynthetic CO<sub>2</sub> fixation in C<sub>3</sub> plants. *Ann. Rev. Plant Physiol. Plant Mol. Biol.* 39, 533–594.
- Xu, M., DeBiase, T.A., Qi, Y., Goldstein, A., Liu, Z., 2001. Ecosystem respiration in a young ponderosa pine plantation in the Sierra Nevada Mountains, California. *Tree Physiol.* 21, 309–318.